AGU ADVANCING EARTH AND SPACE SCIENCES

JGR Earth Surface

RESEARCH ARTICLE
10.1029/2025JF008574

Grain Size Sorting and Steady Bars Formation in Straight Channels—Part 1: Laboratory Experiments

Marco Redolfi[1], Niccolò Ragno[2], Matilde Welber[2], and Walter Bertoldi[2]

[1]Department of Engineering "Enzo Ferrari", University of Modena and Reggio Emilia, Modena, Italy, [2]Department of Civil, Environmental, and Mechanical Engineering, University of Trento, Trento, Italy

Key Points:

- High-resolution maps of grain size and bed elevation over steady bars were captured under diverse experimental conditions
- Correlation analysis reveals recurring patterns, with grain size consistently shifted relative to bed topography and shear stress
- Sorting patterns remain unaffected by changes in discharge and channel width

Correspondence to:

M. Redolfi,
marco.redolfi@unimore.it

Citation:

Redolfi, M., Ragno, N., Welber, M., & Bertoldi, W. (2026). Grain size sorting and steady bars formation in straight channels—Part 1: Laboratory experiments. *Journal of Geophysical Research: Earth Surface*, *131*, e2025JF008574. https://doi.org/10.1029/2025JF008574

Received 9 MAY 2025
Accepted 31 MAY 2026

Author Contributions:

Conceptualization: Marco Redolfi, Niccolò Ragno, Matilde Welber, Walter Bertoldi
Data curation: Marco Redolfi
Formal analysis: Marco Redolfi, Matilde Welber
Funding acquisition: Marco Redolfi, Walter Bertoldi
Investigation: Matilde Welber
Methodology: Marco Redolfi, Niccolò Ragno, Matilde Welber, Walter Bertoldi
Project administration: Marco Redolfi, Walter Bertoldi
Resources: Walter Bertoldi
Software: Marco Redolfi, Matilde Welber, Walter Bertoldi
Supervision: Matilde Welber, Walter Bertoldi
Validation: Marco Redolfi, Niccolò Ragno, Matilde Welber, Walter Bertoldi
Visualization: Marco Redolfi

Abstract Surface grain size in gravel-bed rivers is inherently heterogeneous, with marked spatial variability that remains challenging to predict, even in the presence of regular bedforms. This study investigates surface grain size variability on self-formed alternate bars at the scale of a single bar unit, and is divided in two parts. In Part 1, controlled laboratory experiments were conducted in a straight flume with fixed banks under steady water discharge and sediment supply conditions. High-resolution maps of bed topography and surface grain size were created using close-range photogrammetry and automated image analysis, while numerical simulations provided estimates of the flow field and bed shear stress distribution. Experiments show the formation of initially migrating bars, which gradually slow down, eventually leading to a steady configuration. Analysis of this equilibrium state reveals recurring periodic patterns in bed topography, shear stress, and grain size. Coarser sediment patches predominantly occur on the stoss side, upstream of the bar crest, while finer sediments concentrate near the bar front, upstream of pools. Grain size distribution is not directly correlated with bed elevation or bed shear stress but displays a systematic upstream shift with a consistent phase lag across all experiments. These patterns were unaffected by changes in discharge or channel width. Moreover, our analysis shows that the flow deflection induced by bars limits sediment transport on bar tops, which explains the lack of migration and the relatively long bar wavelength. In Part 2, a theoretical model is formulated to provide a mechanistic interpretation of the experimental results.

Plain Language Summary Gravel-bed rivers are characterized by sediments of various sizes, ranging from sand to gravel and cobbles, which move differently and settle in specific locations. This process creates grain size patterns that influence the river's shape and dynamics, making them crucial for understanding sediment transport and predicting river evolution. This study, presented in two related papers, examines how these patterns vary on regular gravel bars, large sequences of alternating scour and deposition zones that naturally form in rivers. In this first paper, we present the outcomes of a series of controlled experiments conducted in a straight laboratory channel. Using advanced imaging tools, we created detailed maps of bed topography and grain size, while numerical simulations were used to reconstruct water flow. The results show that coarse gravel is more likely to deposit on the upstream slopes of bars, while finer sediments accumulate near pools farther downstream. These grain size patterns are not directly linked to bed height but instead appear consistently shifted upstream, forming predictable distributions across different conditions. Over time, the deposition of coarse grains at bar heads alters the flow and slows sediment movement, preventing downstream bar migration and leading to bar elongation.

1. Introduction

Gravel-bed rivers are typically characterized by significant sediment heterogeneity, with surface grain size distributions varying across multiple spatial scales (e.g., Buffington & Montgomery, 1999; Paola & Seal, 1995; Parker, 2008). This variability arises from the adjustment of riverbed composition to changes in flow and bed topography, producing vertical, lateral, and downstream changes in grain size distribution through different grain sorting mechanisms (e.g., Parker, 2008; Powell, 1998). The spatial changes of grain size typically appear in the form of patches of coarser or finer surface bed material. Sorting patches can be associated with various bedforms, including dunes, antidunes, riffles and pools, bedload sheets, longitudinal streaks (Alexander & Fielding, 1997; Colombini & Parker, 1995; Hassan et al., 2022; Hodge et al., 2013; Nelson et al., 2009; Seminara et al., 1996; Whiting et al., 1988). By modifying bed roughness and sediment mobility, such features directly affect flow dynamics and sediment transport processes (e.g., MacKenzie et al., 2018). In addition to their morphological significance, sorting patches provide ecological benefits, increasing habitat diversity, providing ideal substrates

Writing – original draft: Marco Redolfi, Niccolò Ragno, Walter Bertoldi
Writing – review & editing: Marco Redolfi, Niccolò Ragno, Walter Bertoldi

for fish reproduction, and creating favorable conditions for riparian vegetation and benthic species (Garcia et al., 2012; Gurnell et al., 2001; Tockner et al., 2006).

In this work, we focus on sorting patches at the scale of the channel width, as those commonly occurring within meander bends, on river bars, and among branches in multi-thread rivers (e.g., Ashworth et al., 1992; Lisle & Madej, 1992; Storz-Peretz & Laronne, 2013). A key mechanism driving these patterns is gravitational selection, which tends to move larger and heavier particles to lower elevations (Parker & Andrews, 1985; Powell, 1998). This explains why in meander bends coarser grains are typically found in pools, while point bars tend to be finer (Julien & Anthony, 2002; Parker & Andrews, 1985; White & Nelson, 2023). Another key mechanism is the selective transport of different grain-size fractions within a mixture, which appears particularly important in relatively straight reaches (e.g., Lisle et al., 1991; Lisle & Madej, 1992; Nelson et al., 2015a).

The spontaneous formation of bars in relatively straight reaches of gravel-bed rivers is a frequent phenomenon, arising from an intrinsic large-scale, three-dimensional bed instability that governs the morphodynamics of channel bifurcations and drives the development of braided rivers (e.g., Callander, 1969; Colombini et al., 1987; Fredsoe, 1978; Parker, 1976; Seminara, 2010). From a practical perspective, gravel bars can affect navigability, enhance bank erosion, and interact with instream engineering structures (e.g., Claude et al., 2014), and can provide valuable ecosystem services (e.g., Ward et al., 2002).

Gravel bars have been found to form distinct sediment sorting patterns. The most widely reported pattern consists of a grain size gradient, with coarser material at the bar head and finer material at the bar tail (e.g., Ashworth & Ferguson, 1986; Lewin, 1976; Lunt & Bridge, 2004; Rice & Church, 2010). Several studies also observed that fine material tends to accumulate in pools, while bar crests are often coarser (Lanzoni, 2000; Lisle & Madej, 1992; Nelson et al., 2010). However, other studies report contrasting patterns. For instance, experimental and numerical findings by Takebayashi and Egashira (2001), conducted under well-above-threshold transport conditions, revealed a clear coarsening of pools and a fining of crests, nearly opposite to the experimental and numerical results by Nelson et al. (2010, 2015a). Numerical simulations by Cordier et al. (2019) also revealed how stationary bars exhibit a different trend with respect to migrating bars, with the former showing coarsening within bar pools. Finally, Qian et al. (2017) obtained numerically coarser pools and finer crests under partial mobility conditions, while a nearly opposite pattern was found under high mobility conditions.

Evidence of consistent formation of sorting patches around bars also appears in contrast to several investigations showing almost zero correlation between bed elevation and grain size. For example, laboratory experiments by Gardner and Ashmore (2011) and Leduc et al. (2015) showed a poor correlation between elevation and grain size along a braided channel network. Similarly, measurements taken along compound bars of the Fraser River by Rice and Church (2010) revealed no correlation between bed elevation and grain size, although there appears to be a limit on the maximum elevation that coarse particles can attain. Extensive measurements along a reach of the gravel-bed Ashley River by Mosley and Tindale (1985) also highlighted a lack of any obvious relationship between grain size parameters and their location on diagonal bars, transverse bars and pools. Finally, analysis of the surface bed material within the gravel-bedded Urumqi River by Guerit et al. (2014) showed how the grain size range of anabranches and bars is too close to be distinguished, with only the chute channels showing significantly coarser material. The question then arises whether this lack of correlation implies that some river systems are so complex that no systematic patterns can be predicted, or whether consistent patterns can still be identified, possibly not in the form of a direct, pointwise correlation between elevation and grain size.

The lack of a coherent picture emerging from the mentioned works mirrors a lack of understanding of the physical controls underlying the different observations. In particular, it is still unclear how the arrangement of sorting patches is related to the spatial variation of bed shear stress, which is expected to be the main driver of size-selective sediment transport along alternate bars (Lanzoni, 2000). In this context, numerical simulations based on 2-D shallow water equations provided useful information, as they allow detailed mapping of flow field and grain size distribution to be obtained. Using this approach, Cordier et al. (2019) showed that coarser patches forming on the crests of stationary bars correspond to areas of high bed shear stress, suggesting that the surface bed composition is directly related to the flow capacity to transport bed material of varying sizes. In contrast, simulations by Nelson et al. (2015b) indicated that sorting patterns are not directly related to the magnitude of bed shear stress, but rather to its divergence, as also suggested by experimental analysis by Lisle et al. (1991).

In this study, we aim to understand whether the equilibrium state of self-organizing alternate bars is associated with systematic and reproducible sorting patterns, at least under controlled conditions. Moreover, we aim at exploring the spatial arrangement of sorting patches, and their relationship with the bar topography and the associated bed shear stress distribution. The study is divided into two parts. The present manuscript (Part 1) is based on the experimental analysis in a physical laboratory model, while the companion paper (Part 2, Ragno & Redolfi, 2026) presents a more general, mathematical description of the key mechanisms through a linear perturbation analysis. Specifically, in the present Part 1 we performed a series of experiments in a mobile-bed flume, exploring different combinations of flow discharge and channel width, and consequently bar height and length. These experiments allowed us to systematically explore the occurrence and distribution of sorting patterns, leveraging recent experimental methods that enable detailed and extensive measurements of bed topography and median grain size. Additionally, we performed two-dimensional fixed-bed simulations to generate high-resolution spatial maps of flow depth, velocity, and bed shear stress along the bars. A specific, novel analysis of these data allows us to explain the spatial relationship between observed sorting patterns, bed topography and flow field.

2. Method

2.1. Experimental Setup

The experiments were conducted at the Hydraulic Laboratory of the University of Trento in a 25 m long flume. Vertical banks were installed within the flume to create a straight channel with a width of either 40 cm or 60 cm, as illustrated in Figure 1a. Water flow was recirculated using a submerged, software-controlled pump to maintain a constant discharge throughout the experiments. The channel bed was prepared with a 15 cm thick layer of a sand and small gravel mixture, sieved to remove particles finer than 0.5 mm to prevent cohesion effects and system clogging. The grain size distribution varied slightly between the two experimental series, with the narrower channel configuration (width $W = 40\,\text{cm}$) exhibiting a finer distribution, as shown in Figures 1b and 1c. Specifically, the median grain size decreased from 1.29 mm to 1.22 mm, and the geometric standard deviation decreased from 0.77 to 0.75 when comparing the 60 cm and 40 cm channel widths, respectively. These grain size distributions have a sorting coefficient $(\phi_{16} - \phi_{84})/2 \simeq 0.8$ and are thus classified as moderately sorted (Folk & Ward, 1957). To ensure a uniform initial bed composition, the sediment mixture was thoroughly mixed, and the bed surface was leveled to achieve a consistent longitudinal slope of 1%. The same mixture was used for sediment feeding at the upstream end of the flume. The sediment feed rate, controlled with a motorized screw, was constant for each run and was selected to maintain overall equilibrium conditions throughout each experiment, thereby preventing changes in the average longitudinal gradient. The feeding rate was determined through an iterative process based on preliminary experiments. At the downstream end, transported sediments were collected in a tank supported by four load cells, providing continuous measurements of sediment transport flux.

A total of nine experimental conditions were tested, each with a different constant water discharge (Q). Four experiments were conducted with the narrower channel width ($W = 40\,\text{cm}$), referred to as the MW40 series, and five with the wider channel width ($W = 60\,\text{cm}$), referred to as the MW60 series. For the MW40 series, each experiment was repeated twice to verify results reproducibility. The parameters for each experimental run are detailed in Table 1. Each run lasted between approximately 12 and 80 hours, a duration chosen to ensure that the bed morphology reached an equilibrium state, characterized by stable bar wavelength and amplitude. The mean wetted width (W_w) for each experiment was determined by averaging manual measurements of submerged width taken along 22 equally-spaced (0.5 m) cross-sections during the final phase of each run.

At the end of each experiment, after stopping the water flow, the bed surface topography and surface grain size distribution were surveyed using close-range photogrammetry. Vertical images were captured using a Nikon D7100 camera equipped with a fixed 28 mm focal length lens, mounted on a movable carriage. This setup enabled a rapid survey consisting of 150 images (three images per cross-section and 50 rows along the flume length), with approximately 70% side and forward overlap. Ground control points (GCPs) were placed at 25 cross sections spaced 1 m apart along the flume's longitudinal axis. At each cross section, four GCPs were positioned outside of the flume banks at different elevations to minimize collinearity issues, resulting in a total of 100 GCPs. Image processing was performed using the Structure-from-Motion software Agisoft PhotoScan (version 1.2.2, 2294), which generated digital elevation models (DEMs) and rectified image mosaics of the entire flume at a spatial resolution of 0.5 mm (Redolfi et al., 2025). Ground-truthing points were used to assess the accuracy of the DEMs,

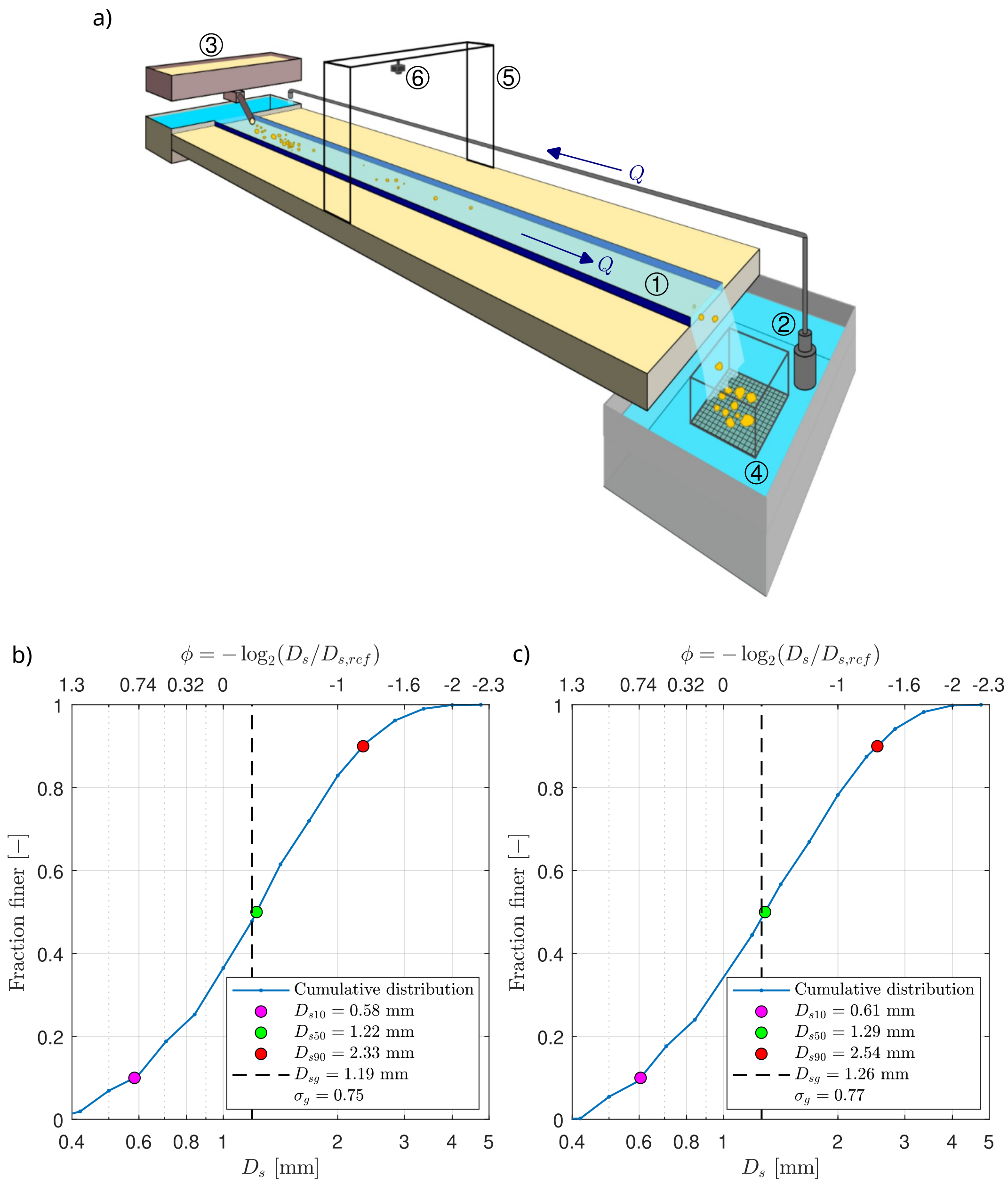

Figure 1. Panel (a): schematic view of the flume experimental setup, showing: (1) the central channel delimited by straight vertical banks; (2) the submerged pump that conveys the water discharge Q (indicated by arrows); (3) the upstream sediment feeder; (4) the downstream sediment collection apparatus; (5) the movable carriage on which the SLR camera (6) is mounted. Panels (b, c): grain size distribution of the sandy mixture employed for MW40 (b) and MW60 (c) experimental series, where D_{s50} (green markers) is the median grain size, D_{s10} (purple markers) and D_{s90} (red markers) are the 10% and 90% percentiles, D_{sg} (vertical dashed line) is the geometrical mean grain size, σ_g is the geometrical standard deviation, and $D_{s,ref}$ is a reference size conventionally set to 1 mm.

yielding a mean absolute error of approximately 2 mm, which is comparable to the bed surface roughness. Further details on the survey method can be found in Javernick et al. (2018). Detrended bed topography was then computed by subtracting a linear elevation profile with uniform slope, resulting in detrended bed elevation maps $\eta(x, y)$, where x and y represent the longitudinal and transverse coordinates, respectively.

Table 1
Summary Data of the Laboratory Experiments, Where S Is the Initial Bed Slope, D_{s50} Is the Median Grain Size, Q Is Water Discharge, Q_s Is the Measured Mean Volumetric Sediment Discharge, and W_w/W Indicate the Measured Ratio Between the Mean Wetted Width and the Flume Width

Exp Id	# Run	W [m]	S	D_{s50} [mm]	Q $[\mathrm{l\,s^{-1}}]$	$\theta(D_{50})$	β	Q_s $[\mathrm{g\,s^{-1}}]$	W_w/W
MW40_Q17	2	0.40	1.0%	1.22	1.7	0.057	17.5	0.62	0.97
MW40_Q20	2	0.40	1.0%	1.22	2.0	0.062	15.9	1.67	1
MW40_Q25	2	0.40	1.0%	1.22	2.5	0.071	14.0	3.14	1
MW40_Q30	2	0.40	1.0%	1.22	3.0	0.079	12.6	4.19	1
MW60_Q30	1	0.60	1.0%	1.29	3.0	0.059	23.8	2.64	–
MW60_Q36	1	0.60	1.0%	1.29	3.6	0.066	21.4	4.68	0.98
MW60_Q42	1	0.60	1.0%	1.29	4.2	0.072	19.5	5.36	0.99
MW60_Q48	1	0.60	1.0%	1.29	4.8	0.078	18.1	7.29	0.98
MW60_Q55	1	0.60	1.0%	1.29	5.5	0.085	16.7	11.02	1

Note. The Shields number relative to the median grain size $\theta(D_{50})$ and the channel aspect ratio β (here defined as half the width-to-depth ratio) are estimated considering a reference uniform flow computed via the logarithmic friction formula 1.

2.2. Grain Size Estimation

The rectified image mosaics were analyzed to estimate the spatial distribution of median grain size. We employed a procedure based on the method proposed by Rubin (2004), which establishes a relationship between grain size and the spatial correlation of image intensity values across various lateral offsets. The underlying principle is that the color within individual sediment particles is relatively uniform, while it varies significantly between different particles. As a result, correlation remains high for offsets shorter than the grain size, while it decreases rapidly for larger offsets. The correlation value at a fixed intermediate offset is therefore expected to increase with grain size. Moreover, in our experiments the larger grains, primarily composed of white carbonate rock, contrasted sharply with the darker, porphyritic sandy component. This color distinction facilitated the identification of grain size variations.

To calibrate the method, images of 24 sediment samples with varying grain size distributions were analyzed. The mean correlation function $(r_{yk} + r_{xk})/2$ was computed as a function of offset k using a 25 mm quadrat window. The optimal offset value for both longitudinal (r_{xk}) and transverse (r_{yk}) directions was determined to be 2 pixels, corresponding to a spatial distance of 1 mm. Two regression relationships were developed to link the mean correlation function to median grain size, depending on the proportion of light-colored pixels p (i.e., pixels with an intensity greater than 130/255). Specifically, samples with $p < 9\%$ and $p \geq 9\%$ were treated separately (see Figure 2a). As illustrated in Figure 2b, this regression provides a mean absolute percentage error in the prediction of D_{s50} of 6.4%. By applying this method to a moving window across the domain, detailed maps of the median surface grain size $D_{s50}(x, y)$ were generated for all experimental runs.

2.3. Hydraulic Modelling

Information about the spatial distribution of water depth, velocity, and bed shear stress was obtained through fixed-bed numerical simulations. We used the two-dimensional software Basement (version 4.0.1), which solves the depth-averaged shallow water equations on an unstructured triangular mesh (Vanzo et al., 2021). For the MW40 and MW60 experiments, two distinct computational meshes were generated with a maximum edge length of 2 cm, resulting in 48164 elements for MW40 and 71656 elements for MW60. The elevation of each mesh element was calculated as the mean value of all measured points falling within the corresponding triangular cell. The rectangular domain was bounded laterally by no-flux boundary conditions. At the upstream end, a constant discharge was prescribed, while at the downstream end a flow rating curve corresponding to critical conditions was imposed to replicate the free-falling flow observed at the flume outlet.

Each simulation was run for 600 s, which was found to be sufficient to achieve a steady-state configuration. Bed roughness was considered to be spatially variable, based on the measured grain size distribution.

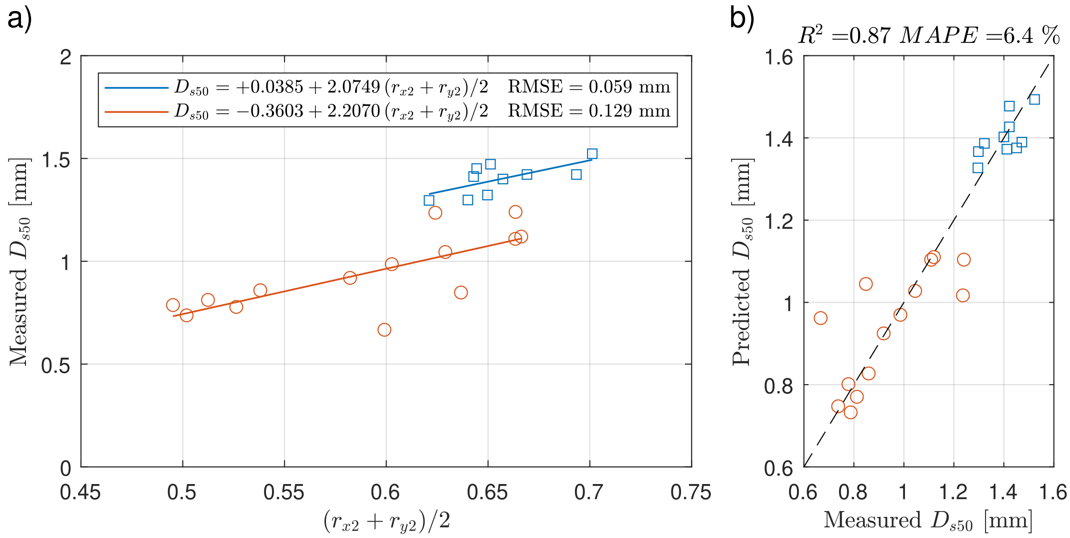

Figure 2. (a) Regression between correlation parameter and measured median grain size D_{s50}, for the two subsets having a percentage of white pixels p higher (blue line and square markers) and lower (red line and circle markers) than the threshold value 0.09. RMSE denotes the root mean square error of the linear regression. (b) Comparison between measurements and prediction from linear regression, with dashed line indicating perfect agreement. R^2 is the coefficient of determination, while *MAPE* indicates the mean absolute percentage error.

Specifically, the dimensionless Chézy parameter (C) was computed using the logarithmic expression proposed by Keulegan (1938):

$$C = 6 + 2.5\,\log\left(\frac{D}{\alpha D_{s50}}\right), \tag{1}$$

where D is the water depth, D_{s50} is the local median grain size, and α is a dimensionless calibration parameter. The value of α was determined through calibration against measurements of the mean wetted width (W_w) in five distinct MW60 experiments. This yielded a value of $\alpha = 1.2$, which was associated with errors in W_w/W of about $1 - 2\%$. The resulting value of α falls within the typical range reported in the literature (e.g., García, 2008).

Resulting maps of the bed shear stress τ allowed for estimating the mobility of different grain sizes by computing Shields number as:

$$\theta(D_s) = \frac{\tau}{g(\rho_s - \rho)D_{s50}}\mathcal{H}_r\left(\frac{D_s}{D_{s50}}\right), \tag{2}$$

where g is the gravitational acceleration, ρ_s and ρ are sediment and water densities, and $\mathcal{H}_r$ is the reduced hiding function, here evaluated using the Wilcock and Crowe (2003) formulation.

2.4. Correlation Analysis

Alternate bars can be interpreted as two-dimensional waves, in which all quantities exhibit periodic repetitions along the longitudinal direction. However, not all flow and bed structure parameters are synchronous, and they may be shifted longitudinally by a specific spatial lag. Quantitative insight into the spatial arrangement of bed topography, median grain size, and bed shear stress can thus be obtained through cross-correlation analysis, which identifies the spatial lag between different quantities.

Considering two generic maps K and Z constituted by a regular grid of $N \times M$ points, we compared the values of K at each point (i,j) with values of Z at $(i + k, j)$, where k is an integer variable representing the spatial *offset* ψ:

$$\psi = k\,dx, \tag{3}$$

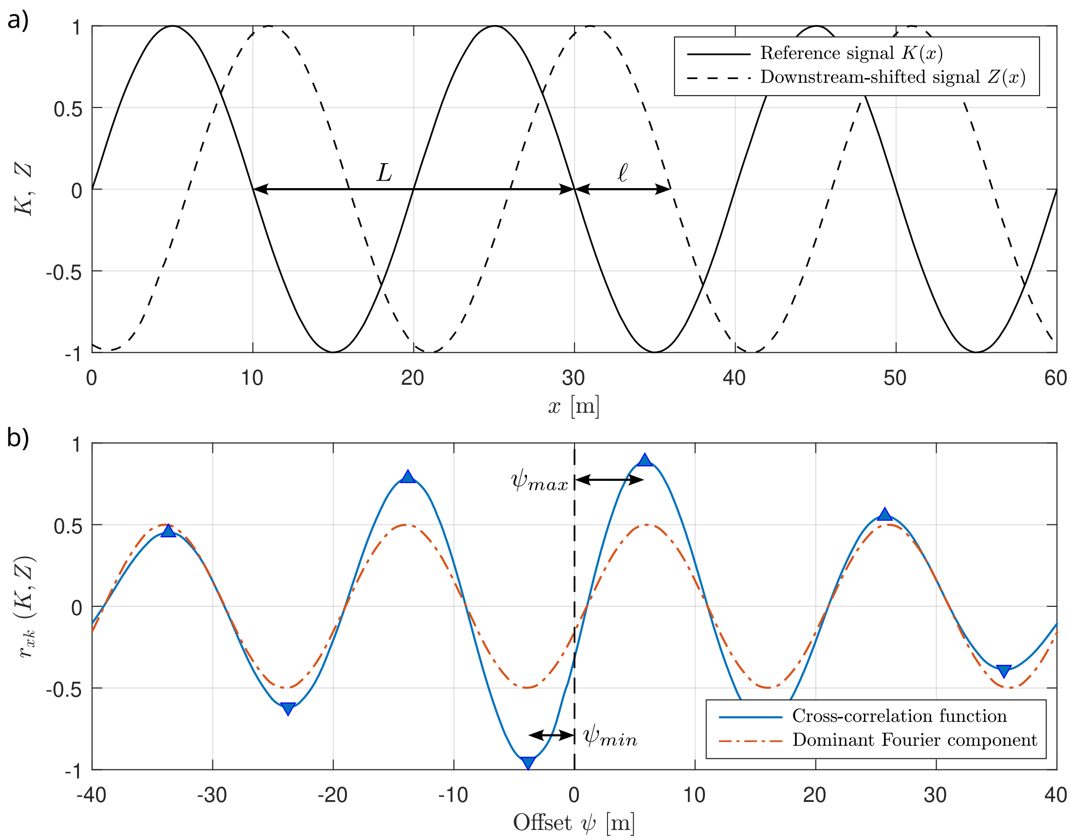

Figure 3. (a) Example of sinusoidal signals K and Z with wavelength L, where Z is shifted downstream by a spatial lag ℓ. (b) Cross-correlation as a function of the offset ψ, where $\psi_{\max}$ represents an estimation of the spatial lag ℓ, while $2|\psi_{\max} - \psi_{\min}|$ estimates the wavelength L. The red dash-dotted line represents the dominant component of the Fourier spectrum, which can also be used to measure both the spatial lag and the wavelength.

with dx indicating the grid spacing

Specifically, the cross-correlation function was computed as:

$$r_{xk}(K,Z) = \begin{cases} \sum_{i=1}^{N-k}\sum_{j=1}^{M} K'_{i,j}Z'_{i+k,j} \Big/ \sum_{i=1}^{N}\sum_{j=1}^{M} K'_{i,j}Z'_{i,j} & k \geq 0 \\ \sum_{i=1}^{N+k}\sum_{j=1}^{M} K'_{i-k,j}Z'_{i,j} \Big/ \sum_{i=1}^{N}\sum_{j=1}^{M} K'_{i,j}Z'_{i,j} & k < 0 \end{cases}, \tag{4}$$

where K' and Z' indicate the maps obtained by subtracting their respective mean values, and the subscript x denotes that the offset is applied in the longitudinal direction. For a simple case where the two maps K and Z are identical but Z is shifted downstream by a spatial lag ℓ, the correlation function, as the offset ψ varies, will reach a maximum when the offset matches the spatial lag $(\psi_{\max} = \ell)$. Thus, identifying changes in correlation across different offsets, particularly the occurrence of a maximum, allows for the determination of whether a consistent spatial lag exists between the two maps.

To illustrate the behavior of the correlation function, consider the example of two periodic sinusoidal waves (Figure 3). In this scenario, the correlation function oscillates with nearly the same period as the waves themselves, such that the distance between consecutive maxima or minima provides an estimate of the wavelength, L. For such wavelike signals, it is useful to define the phase lag, which can be calculated as:

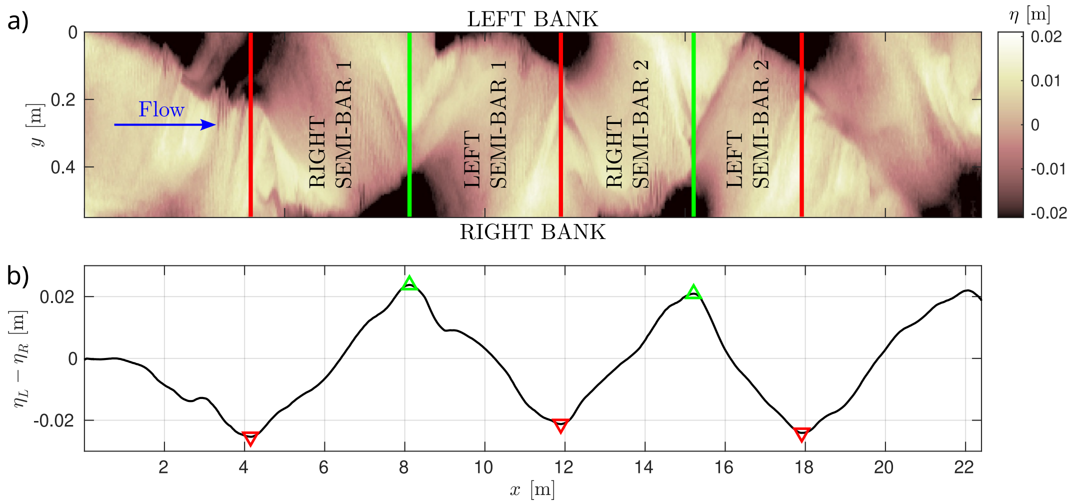

Figure 4. Illustration of the automatic procedure used to identify bar units: (a) topography of the experiment MW60_42, in which the division line among individual semi-bars is positioned on the basis of the extreme values of the signal $\eta_L - \eta_R$ illustrated in panel (b), which represents the difference between the average elevation of the left and the right halves of the channel (smoothed by applying a moving average with a 50 cm window). Left and right semi-bars are conventionally defined depending on whether bar crests start at the left or the right side of the channel.

$$\delta = 2\pi \frac{\ell}{L} = 2\pi \frac{\psi_{\max}}{2|\psi_{\max} - \psi_{\min}|}, \tag{5}$$

where $\psi_{\max}$ and $\psi_{\min}$ are defined as the points where the local maximum and minimum closest to $\psi = 0$ occur, respectively. The phase lag ranges from $-\pi$ ($\psi_{\min} = 0$ and $\psi_{\max} < 0$) to π ($\psi_{\min} = 0$ and $\psi_{\max} > 0$), with a value of zero indicating no lag $(\psi_{\max} = 0)$.

While the above procedure provides a straightforward estimate based on peak locations, a more robust quantification of phase lag and wavelength is obtained using Fourier analysis of the correlation signal. Specifically, we identified the dominant component from the Fourier spectrum, and we computed both the wavelength and the angle of its complex amplitude. To improve the spectral resolution, we padded the r_{xk} signal with a large number ($= 9N$) of zeros, effectively yielding a nearly continuous Fourier transform in the frequency domain. Compared with the peaks analysis presented above, this procedure is less sensitive to noise in the correlation signal, which can slightly shift the position of the nearest maximum and minimum. However, the overall results turn out to be essentially independent of the procedure used to estimate phase lags and wavelengths.

Correlation analysis was performed for all experimental runs to quantify the spatial relationship between median grain size, bed elevation, and bed shear stress. To remove potential reach-scale longitudinal trends and local differences in bar topography, the cross-sectional mean was subtracted from the bed elevation maps.

2.5. Ensemble Analysis

To provide a statistically robust description of the bar unit topography and grain size distribution, we computed the "ensemble bars" following the idea proposed by Redolfi et al. (2020). The method is based on isolating individual bar units, overlapping their topographical map (or other maps), and then computing the average value among all observed bars to obtain a statistical representation of their spatial arrangement.

Differently from Redolfi et al. (2020), here we employed a fully-automated procedure to isolate individual bar units, similar to that proposed by Nelson and Morgan (2018). Our algorithm first calculates the average bed elevation for the left and the right halves of each cross-section (η_L and η_R). Computing their difference and smoothing the resulting signal gives the plot of Figure 4b, in which minimum points represent cross-sections where bar crest is located on the right, while maximum points occur where crest is at the left side. In this way we obtained separation lines among individual semi-bars (Figure 4a), where the prefix "semi" is used to indicate

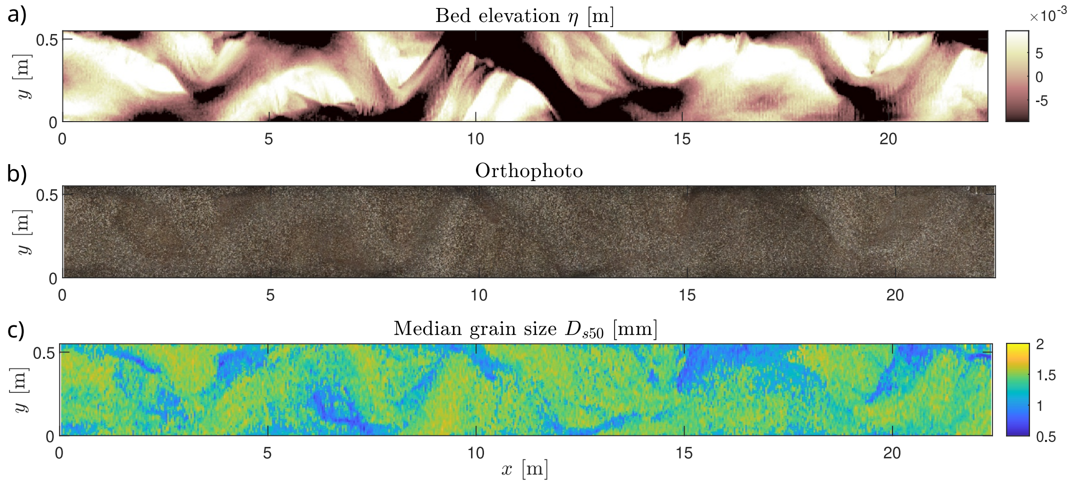

Figure 5. Example of (a) bed topography, (b) RGB orthophoto, and (c) median grain size map for the experiment MW60_Q30. Flow is from left to right. Axes are not in scale (transverse coordinates are magnified by a factor 4). Bed elevation data has been detrended to remove the mean longitudinal slope.

that each unit actually represents half of a bar period. Specifically, we defined left semi-bars as those starting with the crest on the left, and right semi-bars as the others. Within each semi-bar, we then defined a regular sub-grid of (500 × 200 points) and we resampled the map at these grid points. For each point, we then computed the average across all observed left and right semi-bars. In this way, we obtained an average representation for the left and right semi-bars, which were then joined to obtain a complete averaged representation—referred to as *ensemble map*—expressed in normalized coordinates x/L and y/W.

3. Results

3.1. Bed Topography, Grain Size Sorting, and Bed Shear Stress

In all the experiments, an alternating bar pattern spontaneously developed from the initially flat bed. Following an initial transitional phase, the bed configuration reached a quasi-equilibrium state, with the presence of large, non-migrating and irregular alternate bars. Figure 5a illustrates an example of fully developed topography, characterized by relatively flat bar crests and a main sinuous channel that meanders between both sides of the flume.

A clear alternating pattern also appears in the orthophoto shown in Figure 5b, where brighter areas indicate coarser surface material. This spatial distribution is quantified in the median grain size map presented in Figure 5c. At a first sight, finer material appears to accumulate in the deeper sections of the main channel, while coarser material is preferentially located on the bars. This observation suggests a potential correlation between the elevation and the median surface grain size. However, as shown in Figure 6a, data exhibit significant scatter, and no clear relationship between median grain size and bed elevation emerges. This is confirmed by the low value of R^2.

A stronger correlation might be expected when comparing surface composition to bed shear stress, as the latter constitutes an important control on selective transport processes (e.g., Parker, 2008). Figure 7 presents the simulated water depth, bed shear stress, and velocity field for the same experiment, showing that bar crests are almost dry, while water depth in the main channel reaches a few centimeters, and bed shear stress values approach approximately 2 Pa. However, as shown in Figure 6b, the relationship between local bed shear stress and median grain size exhibits again considerable scatter, although a weak positive trend is apparent.

3.2. Correlation and Associated Spatial Lags

The lack of a point-by-point correlation (Figure 6), combined with the observation that similar spatial arrangements can be identified from the maps of topography, grain-size, and bed shear stress (Figures 5 and 7), suggested an investigation into the occurrence of spatial lags between these signals. The correlation function between bed elevation η and median grain size D_{s50} for varying offset values is reported in Figure 8a. This function closely

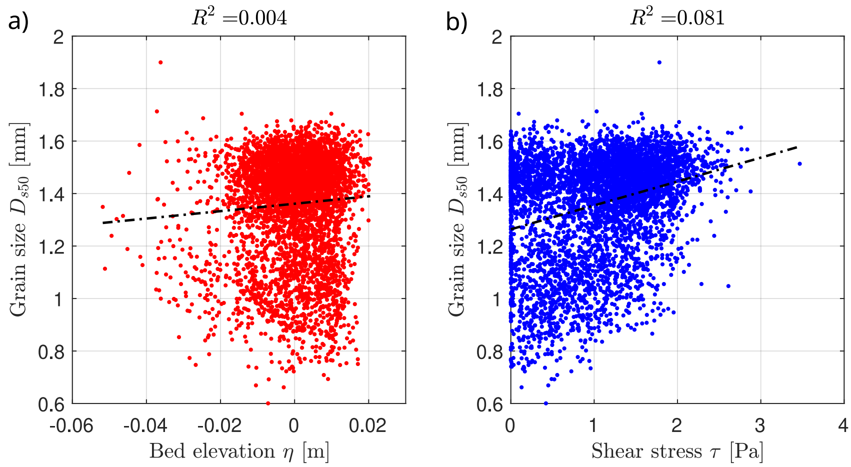

Figure 6. Scatter plot illustrating how the median grain size is related to local values of (a) bed elevation and (b) bed shear stress for the experiment MW60_Q30. The dash-dotted lines represent the linear interpolations, with R^2 indicating the coefficients of determination.

resembles the example in Figure 3, suggesting that the observed bed topography can be effectively characterized as a wave-like phenomenon with a distinct wavelength. This result is expected, as bars are known to form due to an instability mechanism that, in its simplest form, can be represented as a double sinusoid in the longitudinal and transversal directions (e.g., Colombini et al., 1987; Parker, 1976). However, it is notable that this fundamental wave pattern can be clearly extracted from the correlation of inherently noisy and irregular maps. A similar correlation function was observed across all experimental runs, enabling consistent estimation of bar wavelength and spatial lag. Figure 8b illustrates the wavelengths for all runs, which range from approximately 9 to 17 times the channel width. An overall trend emerges, showing that wavelength increases with increasing unit discharge (p-values < 0.01 for both experimental series) and decreasing channel width.

The correlation peak in Figure 8a is not centered at $\psi = 0$, but instead occurs at negative offset values, indicating that the median grain size maps are shifted upstream relative to the bed topography. Figure 9a reveals that the spatial lag ℓ between bed elevation and median grain size is consistently negative, with values ranging from approximately -0.8 m to -2.2 m. Additionally, the spatial lag appears to slightly decrease with decreasing channel width and with increasing unit discharge (p-values of 0.02 and 0.37 for the MW40 and MW60 series, respectively). In terms of phase lag, the results are highly consistent across experiments (Figure 9c). Specifically, the phase lag δ lies within a relatively narrow range, approximately from $-\pi/4$ to $-\pi/2$, with no discernible trend related to unit discharge (p-values 0.51 and 0.83) or channel width.

Using the same procedure, we analyzed the correlation between bed elevation and bed shear stress. As illustrated in Figure 9b, values of the spatial lag ℓ are consistently negative, ranging from about -1 m to -3.5 m and

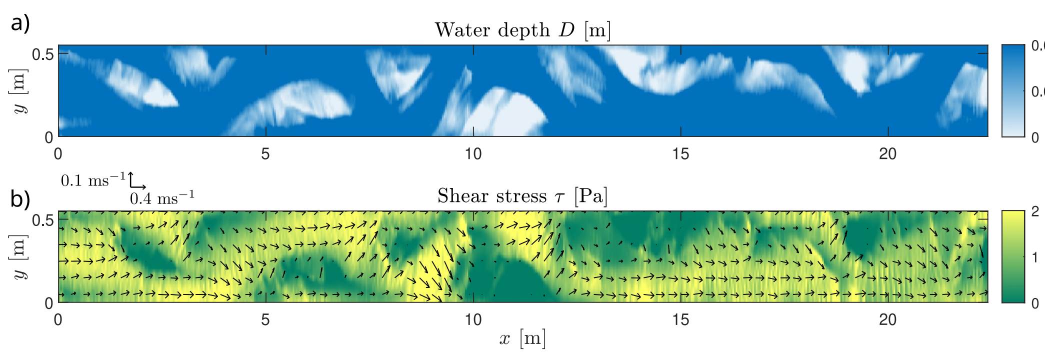

Figure 7. Simulated (a) water depth and (b) bed shear stress with superimposed velocity field (arrows) for the experiment MW60_Q30. Flow is from left to right. Axes are not in scale (transverse coordinates are magnified by a factor 4).

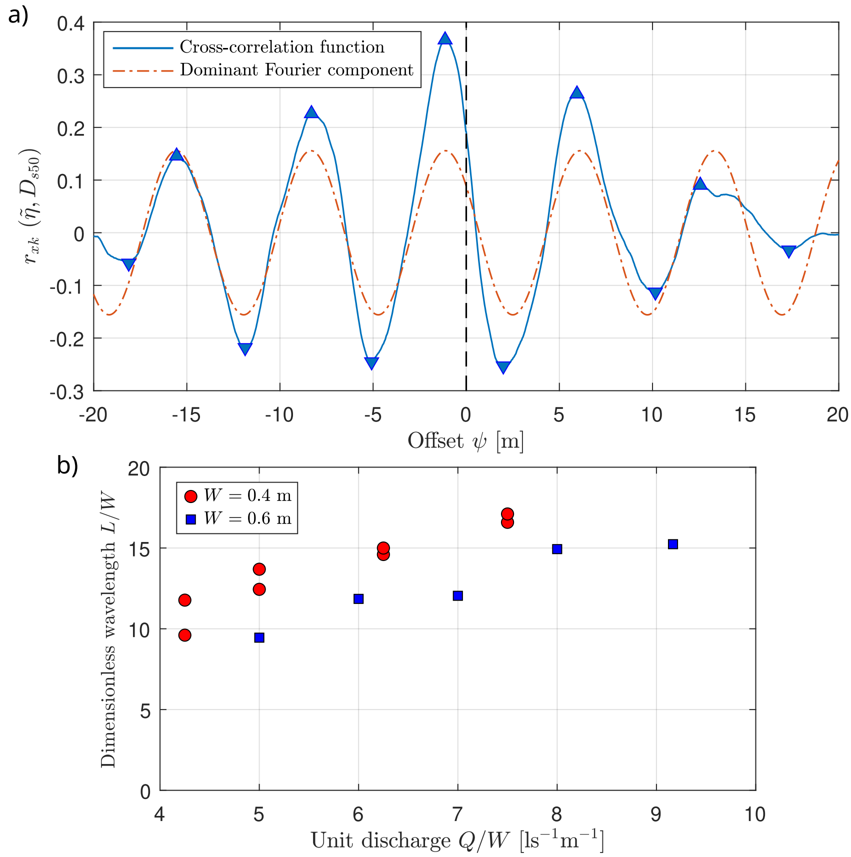

Figure 8. (a) Correlation between bed elevation and median grain size as a function of the offset, shown for the experiment MW60_42. Triangles indicate the peak correlation values, while the red dash-dotted sinusoidal line represents the dominant Fourier component of the signal. (b) Bar wavelength for all experiments, calculated as the wavelength of the dominant Fourier component.

significantly decreasing with discharge (p-values < 0.01 and 0.02 for MW40 and M60 experiments, respectively). Moreover, values of ℓ are lower than those observed for the correlation between bed topography and grain size maps (Figure 9a). The corresponding phase lag varies between $-\pi$ and $-\pi/2$, indicating an upstream shift of half to a full wavelength (Figure 9d). Noteworthy, as in Figure 9c, no significant trends with discharge (p-values of 0.91 for both series) can be detected. These findings reveal that neither median grain size nor bed shear stress are in phase with bed elevation, with bed shear stress consistently shifted further upstream.

Finally, it is worth highlighting that the maximum correlation value in Figure 8a generally remains below 0.5, indicating that a simple longitudinal shift is not sufficient to fully align the maps. Such alignment would only occur in the presence of a linear relationship between the variables. This limited correlation can be attributed to: (a) irregular bar shapes and variable wavelengths along the channel, (b) localized effects on sediment transport and grain size patterns, and (c) potential measurement errors, particularly in the automatic procedure for the grain size estimation.

3.3. The Ensemble Configuration

A comprehensive and direct description of the average spatial arrangement of grain size along the bars is provided by the ensemble analysis, with results shown in Figures 10 and 11. To enhance visualization of the overall pattern, contour lines and maximum points are overlaid after smoothing the images with a Gaussian filter using a kernel with a standard deviation of 50 pixels. The resulting patterns reveal an almost regular alternating structure: the left ($x/L < 0.5$) and right ($x/L > 0.5$) ensemble semi-bars are nearly identical, but mirrored across the channel centerline. The dashed contours, representing the mean value, enclose nearly half of the area in the median grain size maps D_{s50}, but a larger area in the bed elevation maps η. This suggests that the distribution of bed elevation is

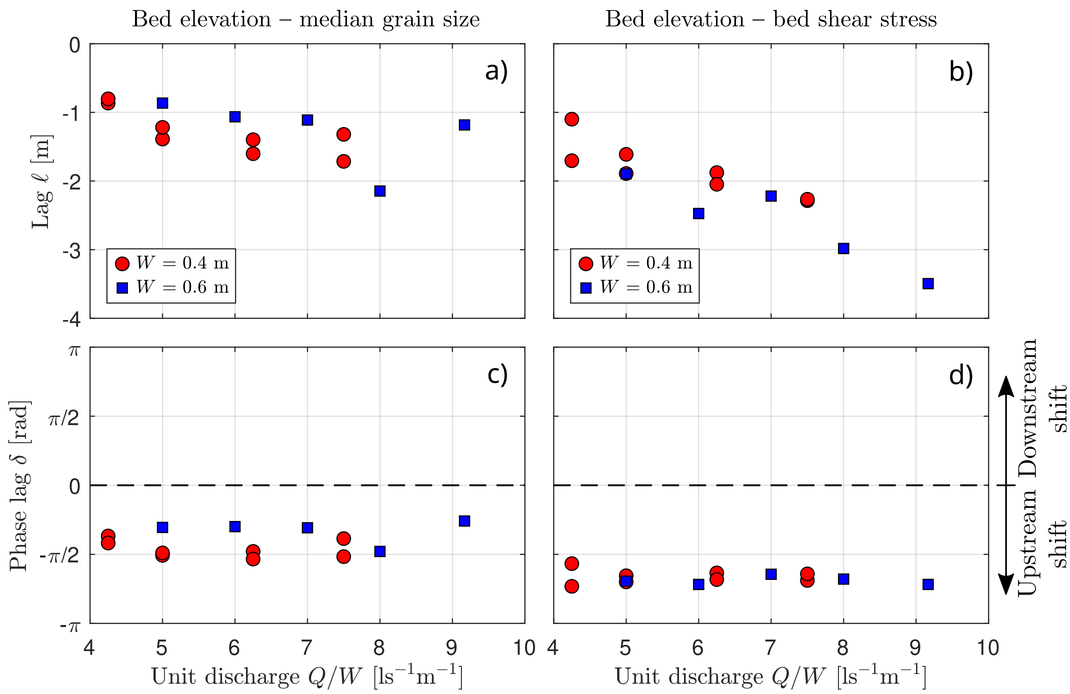

Figure 9. Spatial lag (upper panels) and phase lag (lower panels) between bed elevation and median grain size (left panels) and between bed elevation and bed shear stress (right panels), for all the experiments. Negative values indicate that median grain size or bed shear stress maps are shifted upstream relative to bed topography.

more negatively skewed compared to that of median grain size. Bar crests (points of highest bed elevation) and bar pools (deepest points) are consistently located near the channel banks. Similarly, in the median grain size maps, coarse patches and fine patches also tend to occur near the banks. However, an exception is observed in the MW60 experiment with $Q = 3.6 \text{ls}^{-1}$, where the central channel area appears slightly coarser than the sides. Coarse patches are consistently located just upstream of the bar crests (on the stoss side), while fine patches are located upstream of the bar pools (on the lee side), aligning with the bar front. Overall, the results are consistent with the correlation analysis, confirming a systematic upstream shift of the median grain size maps relative to bed topography, a pattern observed across all experiments.

In Figures 10 and 11 it is also evident that the points of minimum and maximum bed elevations are approximately aligned along the same cross-section, but located on opposite sides of the channel. In contrast, the positions of minimum and maximum surface grain size appear staggered, with fine patches found upstream of the corresponding coarse patches. Consequently, when cross-sectional averages are computed, the extreme values of bed elevation tend to cancel out, whereas the surface grain size retains its variability. This effect is further highlighted through 1-D profiles derived by normalizing the ensemble quantities - that is, subtracting the mean and dividing by the standard deviation - and performing lateral or longitudinal averaging to produce longitudinal profiles $\overline{\eta}(x)$ and transverse profiles $\overline{\eta}(y)$. The longitudinal profiles shown in Figure 12 display a clear double periodicity, directly reflecting the alternating nature of the spatial pattern. Moreover, they appear rather symmetrical with respect to a flipping of the x-axis. The longitudinal profiles of bed elevation (Figure 12a) show minimal variation across different runs, with minor differences in elevation range. In contrast, the longitudinal profiles of surface grain size (Figure 12b) display larger oscillations: while the amplitude remains similar across experiments, the locations of the maxima and minima vary slightly. The peak of $\overline{\eta}(x)$ does not coincide with the bar crests but is instead located midway between crests and pools. Interestingly, the opposite trend is observed in the longitudinally-averaged transverse profiles (Figures 12c and 12d). The bed elevation follows a pronounced bell-shaped profile, with scouring concentrated near the channel banks. On the other hand, variations in surface grain size are more subdued, although a general coarsening trend toward the channel center is observed.

Finally, the ensemble topography was used to calculate the bar height H_{BM}, defined as the difference between maximum and minimum bed elevation. As shown in Figure 13a, bar height decreases with increasing water

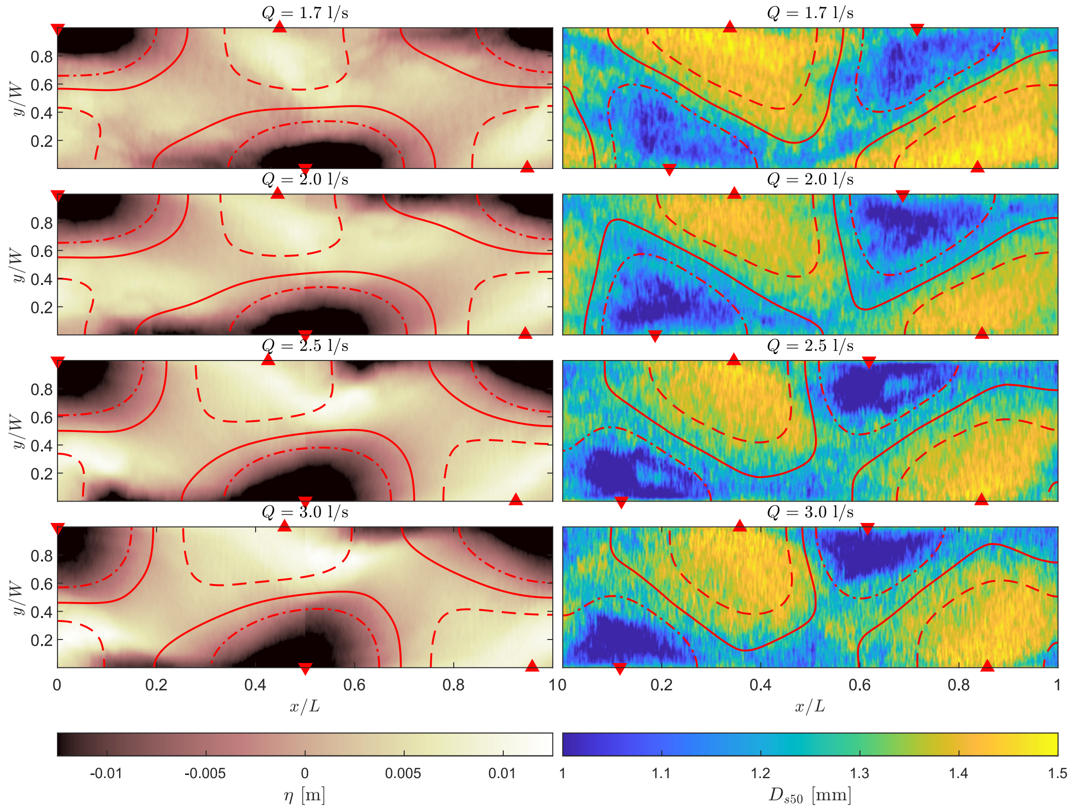

Figure 10. Ensemble bar topography and grain size pattern for the experimental series MW40. Upward and downward triangular markers indicate points of maximum and minimum, respectively; solid contours represent the mean value, while dashed and dash-dotted contours correspond to half a standard deviation above and below the mean, respectively. Flow is from left to right.

discharge, whereas it increases with channel width. This trend can be explained by considering the channel aspect ratio as the primary controlling parameter (e.g., Colombini et al., 1987), with higher aspect ratios associated with relatively taller bars (Figure 13b). Notably, the data point with higher aspect ratio in Figure 13b deviates from this relationship. Rather than representing an outlier, this point likely reflects a reversal of the trend when bars emerge significantly above the water surface, as described by Redolfi et al. (2020). Excluding this point, for all the data series of Figures 13a and 13b linear regression provides p-values < 0.01.

4. Discussion

4.1. Relationship Between Bed Surface Composition and Bar Topography

Sorting of bed material is clearly not essential for the formation of bar patterns, as similar bedforms can be observed even in experiments with nearly uniform grain size. This marks a clear difference with bedforms that are generated or dominated by sediment sorting such as bedload sheets, longitudinal streaks, and sand ridges, as discussed by Seminara (1995). From a top-down hierarchical perspective, the formation of sorting patches along bars can therefore be considered as a secondary effect, where bed topography is primary driver, while sediment sorting mainly arises as a consequence. Nonetheless, grain sorting remains important in controlling quantitative bar properties such as height, wavelength, and migration rate. In this sense, according to Seminara (1995), alternate bars can be considered *sorting-influenced* bedforms.

The experimental results reveal a systematic response of median grain size to the alternate bed topography, despite the inherent complexity of the bed surface composition. However, this relationship does not take the form of a direct correlation between median grain size and bed elevation. Instead, a systematic lag is observed between the peaks of these two variables. This finding aligns with the observations of Milne (1982), who investigated

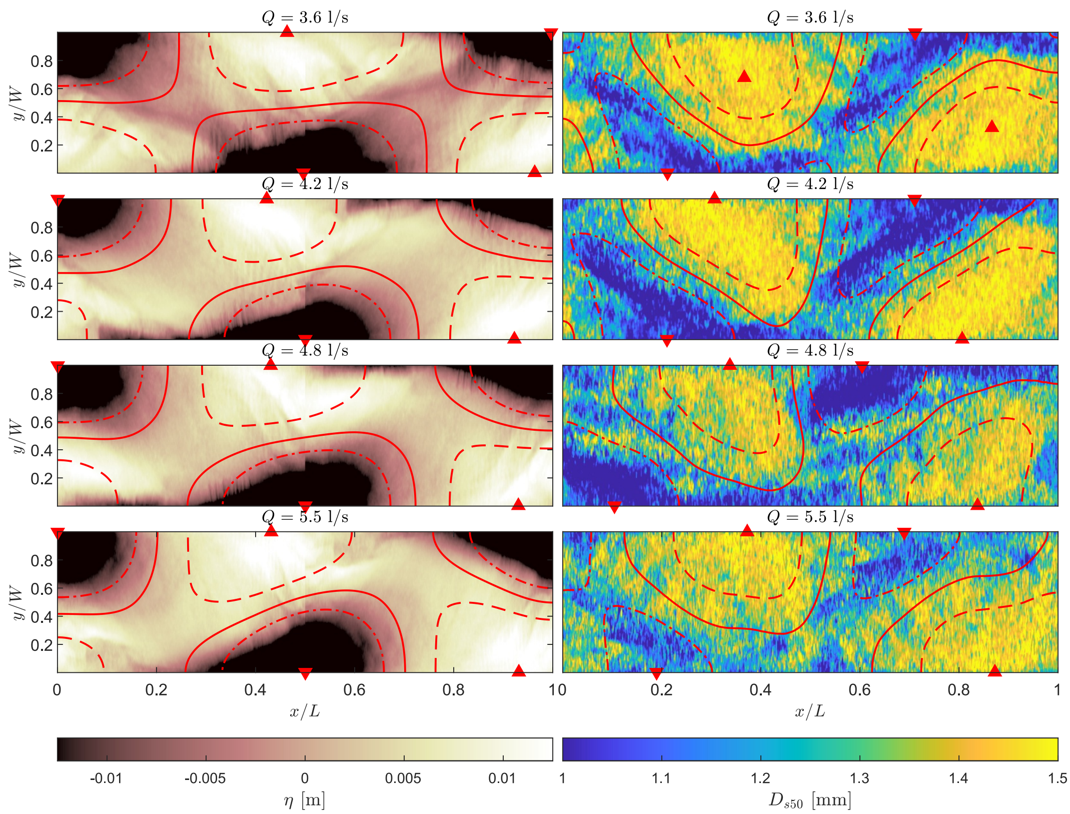

Figure 11. Ensemble bar topography and grain size pattern for the experimental series MW60. Upward and downward triangular markers indicate points of maximum and minimum, respectively; solid contours represent the mean value, while dashed and dash-dotted contours correspond to half a standard deviation above and below the mean, respectively. Flow is from left to right.

cross-sectional variability of grain size within riffle and pool sequences and reported that bed material tends to coarsen approximately 5–7.5 m downstream of the pool.

The emergence of a lag explains why the presence of a clear sorting pattern is not necessarily in contrast to the lack of correlation between grain size and bed elevation. Specifically, the observed phase lag is close to the quadrature of phase ($\delta = -\pi/2$), which represents the exact configuration that minimizes the correlation between the two quantities. In more physical terms, the coarser sediment is preferentially located neither in the pool nor in the crest, but rather at intermediate elevations. Therefore, when assessing grain size relative to average bed elevation, no systematic trend of coarsening or fining is expected.

Our findings appear to be qualitatively consistent with the experimental results of Lisle et al. (1991), which reported deposition of coarse particles at the upstream edges of bar deposits. On the other hand, they differ from the results of both Nelson et al. (2010), who observed coarser bar tops and finer pools, and Takebayashi and Egashira (2001), who noticed almost the opposite pattern. However, grain size data reported by Nelson et al. (2010) do not provide a clear picture of the sorting pattern, particularly near the pool, which makes it difficult to identify the presence of potential lags, especially considering that only data of a single bar unit are available. The grain size mapping by Takebayashi and Egashira (2001) appears clearer. In this case, the different pattern may be explained considering the relatively high values of Shields number, which are expected to reduce differences in mobility between coarse and fine grains (e.g., Parker, 2008). Similarly to Nelson et al. (2010), experiments by Lanzoni (2000) also reported an overall coarsening of bar tops. However, in those experiments, bars were migrating downstream, as opposed to the steady bars reproduced in our experiments. As clearly highlighted by Cordier et al. (2019), freely migrating bars tend to form sharp fronts, with coarse patches located at the bar top, thus with a sorting pattern that is shifted downstream compared to the case of steady bars.

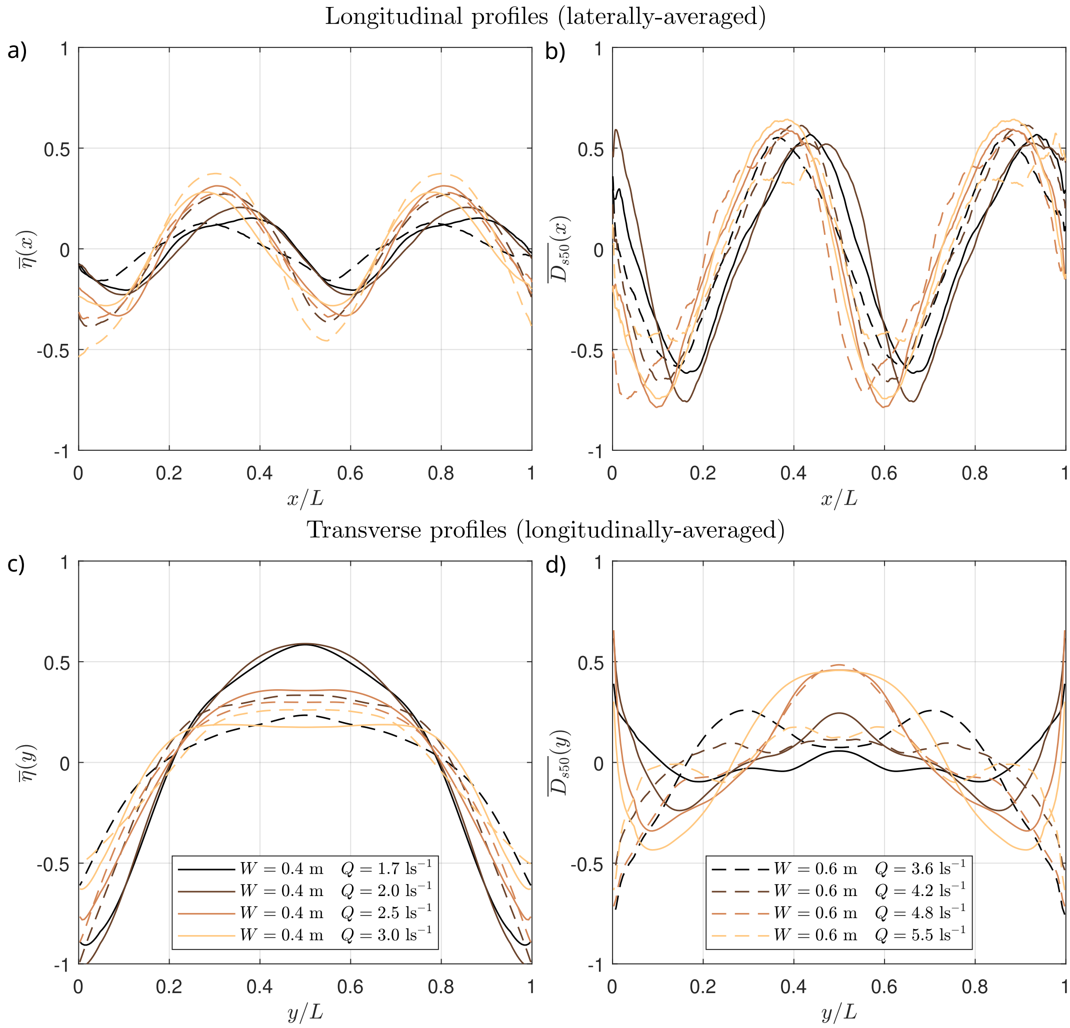

Figure 12. One dimensional profiles of the bed elevation (left panels) and surface grain size (right panels). Upper panels (a, b) report the cross-sectionally averaged, longitudinal profiles, while lower panels (c, d) illustrate the longitudinally-averaged, transverse profiles. To make the variations comparable, profiles are rescaled by removing the global mean and dividing by the standard deviation of the original maps.

The poor correlation observed between median grain size and simulated bed shear stress contrasts with the numerical results of Cordier et al. (2019), which showed systematic fining in low bed shear stress areas and coarsening in high shear stress areas. Instead, our findings are consistent with the field measurements of Lisle et al. (2000), who reported no significant correlation between bed shear stress and surface grain size in gravel-bed rivers with alternate bars. They attributed this lack of correlation to stage-dependent adjustments in surface particle size driven by temporal variations in the bed shear stress field. However, this explanation clashes with our results, as the experiments were conducted under constant discharge conditions. Similarly to the previous observations on the relationship with the bed elevation, we attribute the absence of direct correlation between grain size and shear stress not to the lack of a regular pattern, but rather to the occurrence of a phase lag, which indicates an upstream shift of the bed shear stress signal relative to grain size.

Rice and Church (2010) documented significant grain size variations at the bar scale in the Fraser River, Canada, often exceeding the magnitude of downstream fining observed at the reach scale. Their observations of down-bar fining—characterized by coarser particles upstream and along bar edges—can be partially explained by our finding that surface grain size patterns respond to the topographic forcing exerted by alternate bars with an upstream shift. However, grain size patterns were found to be more complex on compound bars and in areas where secondary unit bars and bar-top channels were present. Complex morphological settings, such as braided

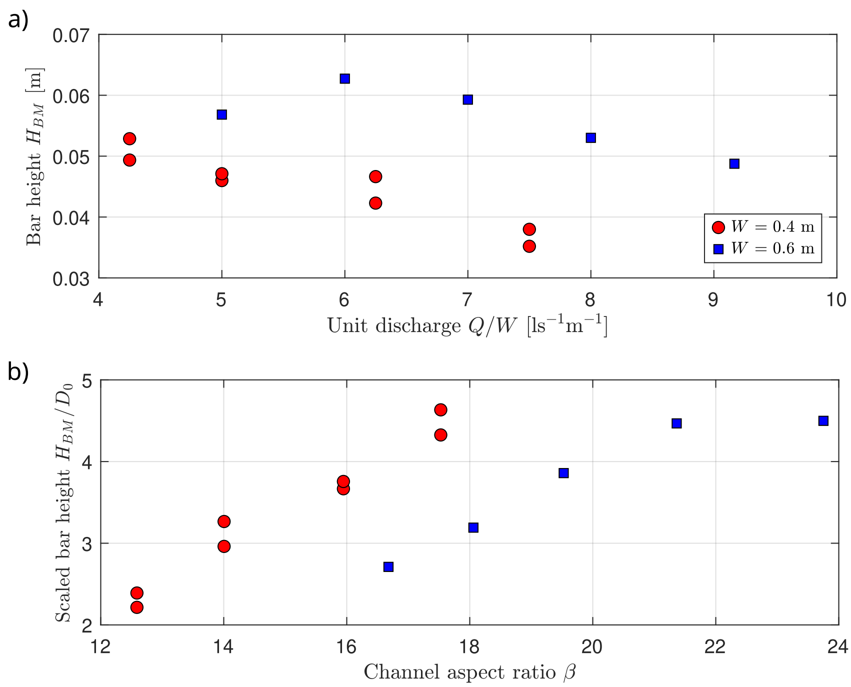

Figure 13. (a) Bar height (H_{BM}) as a function of unit discharge (Q/W). (b) Dimensionless bar height (scaled with the estimated uniform water depth D_0) as a function of channel aspect ratio $\beta = W/(2D_0)$.

rivers, often show little correlation between grain size, bed elevation, and bed shear stress (Leduc et al., 2015). The surface composition in these systems may appear random due to the interplay of various processes across multiple spatial scales. Nevertheless, our results suggest that a spatial relationship between topography and grain size may exist in the form of patches that are consistently shifted with respect to bars.

Furthermore, our experimental observations offer insight into the contrasting grain size distributions observed in relatively straight reaches with bars as opposed to meandering reaches. In meander bends, the bed surface tends to be markedly coarser in pools (e.g., Bluck, 1971; Ikeda et al., 1987; Parker & Andrews, 1985; White & Nelson, 2023), where coarser grains accumulate in depressions—similar to the sorting observed also in scour zones at channel confluences (e.g., Ashmore & Gardner, 2008; Ashworth et al., 1992). This sorting mechanism operates most effectively when sediment transport is mainly governed by secondary flows and gravitational effects. Conversely, in low-sinuosity reaches with alternate bars, the morphodynamics is primarily controlled by flow inertia and gravity, while the role of secondary flows is comparatively weaker (Redolfi, 2021), leading to distinctly different sorting patterns.

4.2. A Physical Explanation of the Bed Shear Stress Lag

The observed phase lags between bed topography, bed shear stress, and median grain size illustrated in Figure 9 remained relatively constant across the analyzed range of conditions. This can be explained by considering that flow velocity, bed shear stress, and sediment flux gradients are expected to depend mainly on the position along the bar, rather than on reference flow parameters, such as channel the aspect ratio β and the Shields number θ (see Table 1). In order to elaborate more on this reasoning, we follow a derivation starting from the standard equation of conservation of depth-averaged longitudinal momentum, and then introducing proper simplifying assumptions. Under steady conditions, momentum conservation reads:

$$\rho D U \frac{\partial U}{\partial x} + \rho D V \frac{\partial U}{\partial y} = -\rho g D \frac{\partial H}{\partial x} + \tau_x, \tag{6}$$

where H is the water surface elevation, and U and V are the depth-averaged flow velocity components in the longitudinal and lateral directions, respectively. Considering a spatially uniform Chézy coefficient C_0, the bed shear stress is calculated as:

$$\tau_x = -\rho \frac{U\sqrt{U^2 + V^2}}{C_0^2}. \tag{7}$$

We then assume the free surface to have a uniform inclination (i.e., neglecting free surface deformation), consistently with previous models of bar dynamics in straight and meandering channels (Camporeale et al., 2007; Struiksma & Crosato, 1989). As discussed by Redolfi (2021), this assumption is justified by the distinctive characteristics of three dimensional bedforms with a length scale several times the channel width, where the flow gently circumvents bars without significantly deforming the free surface. It follows that:

$$\frac{\partial H}{\partial x} = -S_0. \tag{8}$$

Equation 6 can be linearized by considering a small perturbation (denoted with the subscript 1) relative to an undisturbed uniform flow on a plane bed (subscript 0), namely:

$$U = U_0 + U_1, \tag{9a}$$

$$V = 0 + V_1, \tag{9b}$$

$$D = D_0 - \eta_1, \tag{9c}$$

where it is noted that the depth perturbation is exactly equal and opposite to the bed perturbation (i.e., $D_1 = -\eta_1$). At the leading order we get the following uniform-flow relation:

$$g D_0 S_0 = \frac{U_0^2}{C_0^2}, \tag{10}$$

while at the linear level, we obtain:

$$C_0^2 D_0 \frac{\partial U_1}{\partial x} = -\frac{U_0}{D_0}\eta_1 - 2U_1. \tag{11}$$

We now consider purely sinusoidal variations along the longitudinal direction, which can be generally expressed using the following complex exponential notation:

$$U_1 = \hat{u} \exp\left(\frac{2\pi i x}{L}\right) + c.c., \tag{12a}$$

$$\eta_1 = \hat{\eta} \exp\left(\frac{2\pi i x}{L}\right) + c.c., \tag{12b}$$

where $\hat{u}$ and $\hat{\eta}$ are complex coefficients, and c.c. denotes the complex conjugate. Substituting Equation 12 into the linearized momentum Equation 11 gives:

$$\hat{u} = -\hat{\eta} \frac{U_0}{D_0} \frac{1}{(2 + 2\pi i / L^*)}, \tag{13}$$

where the dimensionless length L^* is defined as:

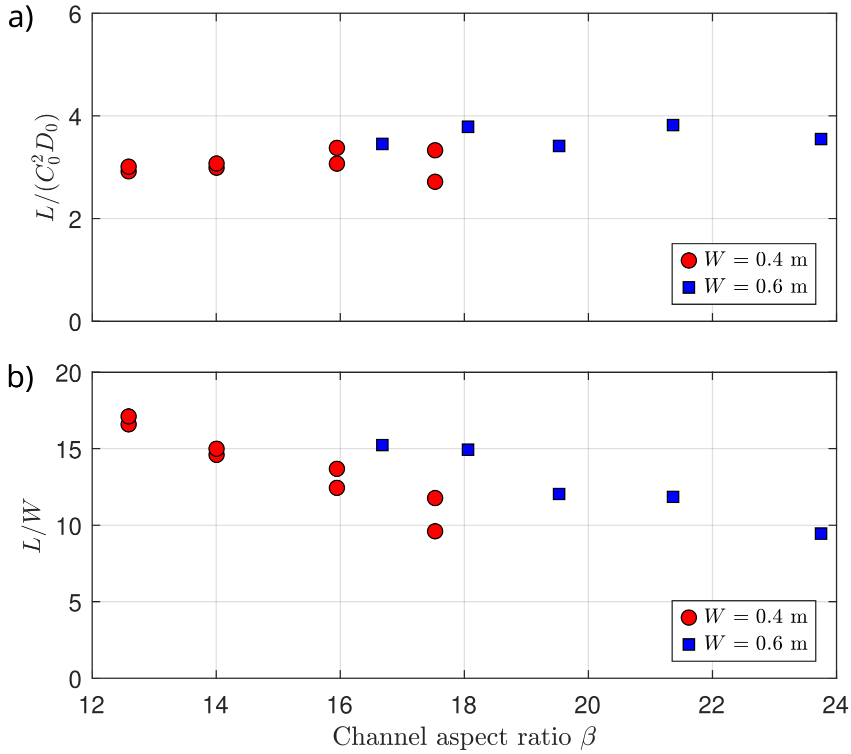

Figure 14. Bar wavelength as a function of channel aspect ratio ($\beta = W/(2D_0)$) for all experiments, scaled by (a) the quantity $C_0^2 D_0$ and (b) the channel width W.

$$L^* = \frac{L}{C_0^2 D_0}. \tag{14}$$

Equation 13 highlights the relationship between the perturbation of bed elevation and water velocity. Information about the phase are contained in the argument of the complex numbers. Specifically, the phase lag is given by:

$$\delta = -\arg\left(\frac{\hat{u}}{\hat{\eta}}\right) = -\pi + \arctan\left(\frac{\pi}{L^*}\right). \tag{15}$$

This analysis shows that the phase lag between bed elevation and velocity waves merely depends on the scaled wavelength L^*. The result becomes particularly interesting when looking at Figure 14a, showing how the experimental values of L^* are essentially constant, which implies that the predicted phase lag δ is also invariant (p-values of 0.82 and 0.52 for the MW40 and MW60 experimental series respectively). Values of the scaled wavelength range approximately from 2.8 to 3.8, which, according to Equation 15, correspond to phase lags from -0.73π to -0.78π, consistent with the observed values around $-3/4\pi$. This is markedly different from result of Figure 14b, where both series show a negative trend of L/W with β (p-values ≤ 0.01). Notably, the scaling quantity $C_0^2 D_0$ brings a clear physical meaning: it represents the spatial scale at which flow inertia and friction becomes comparable, and it has proven to be relevant for a variety of fluvial processes (e.g., Ragno et al., 2022; Struiksma et al., 1985).

It is worth noting that, in reality, perturbations are not small, and the longitudinal variation is not exactly sinusoidal as in Equation 12. However, this first-order representation is sufficient, as a first approximation, to explain why the phase lag of Shields stress is observed to be nearly constant. Similarly, this helps to explain why the lag of median grain size is also found to be constant, considering the dependency of transport processes on Shields stress and bed slope.

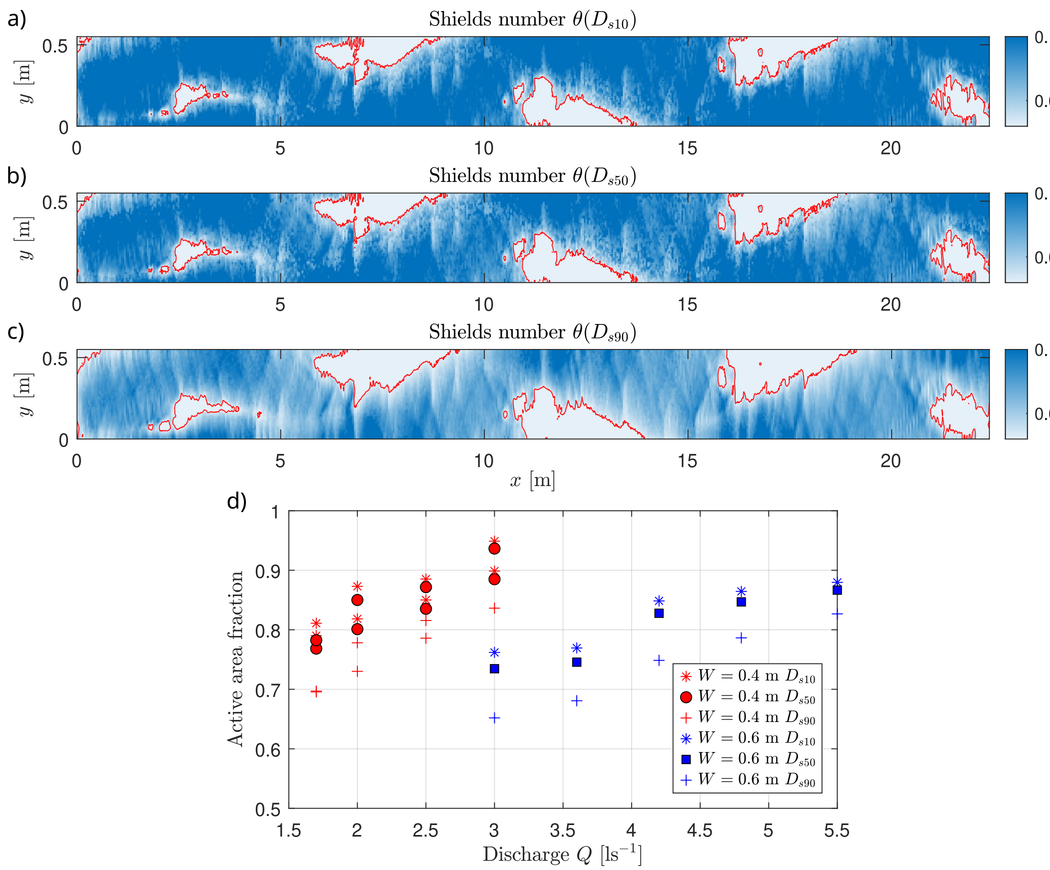

Figure 15. (a, b, c) Maps of Shields number for Experiment MW60_Q55, with the red contour encompassing area with $\theta < 0.03$, where sediment transport is expected to vanish. (d) Percentage of active area ($\theta > 0.03$) for all experiments, calculated with reference to fine, median and coarse grain sizes. While uniform values D_{s10} and D_{s90} are taken from the analysis of Figures 1b and 1c, the median grain size D_{s50} is considered to spatially vary as estimated from image analysis. However, we found that considering spatially uniform values D_{s50} provides almost the same results.

4.3. Effects of Sorting on Bar Morphodynamics

In our experiments, alternating bars developed freely from an initially flat bed without obstructions or other external disturbances. Unlike typical "free bars", these bars exhibited minimal downstream migration, at least during the mature stage of their development. Consequently, they may be considered "free, non-migrating bars", similarly to those observed in tidal channels (Ragno et al., 2021; Seminara & Tubino, 2001).

A similar reduction in bar migration was reported in other experiments involving sediment mixtures (Lanzoni, 2000; Lisle et al., 1991; Nelson et al., 2010; Venditti et al., 2012). Several explanations have been proposed. The analytical model of Lanzoni and Tubino (1999) suggests that sediment heterogeneity generally dampens both the growth rate and migration speed of bars, even during the early stages of their development from an initially flat bed. In addition, the reduction in bed shear stress over the top of developing bars can locally inhibit bedload transport, especially when accompanied by local surface coarsening. For instance, Lisle et al. (1991) attributed the reduction in bar migration speed to the deposition of coarse grains at bar heads, which deflects the flow around the bar, suppresses bedload transport over the bar top, enhances bar emergence, and likely prevents downstream migration.

It therefore seems reasonable to assume that bar migration ceases when bars can no longer transport sediments across their surface. To examine sediment transport conditions in our experiments, we analyzed the spatial distribution of Shields number resulting from numerical simulations, calculated using Equation 2. The results reported in Figure 15 show that, although the average Shields number remains well above the critical value (see Table 1), the reduction in bed shear stress over fully-developed bars renders large portions of the bed near bar tops unable to transport sediment. While the active (i.e., transporting) area increases with discharge, especially in the narrower-width configuration, in all runs except MW40_Q30 there is at least 10% of the surface area where the bed shear stress is insufficient to mobilize even the finer fraction (D_{s10}).

A similar behavior likely occurred in the experiments of Venditti et al. (2012) and in those by Nelson et al. (2010), both of which documented a gradual slowdown of bar migration leading to complete arrest. In both cases, the Shields number was relatively low, with average values below twice the critical threshold. Conversely, in the experiments of Lanzoni (2000) the Shields number of the reference flow was much higher, which explains why in several runs bar migration persisted over the long term. For experiments conducted at lower bed shear stress, however, bar migration eventually ceased; those cases were found to fall within the partial-transport regime, where the coarsest grains remain immobile. Persistent bar migration was also observed by Nelson and Morgan (2018), where the Shields number of the reference flow was nearly twice the critical threshold for sediment motion.

In addition, it is worth mentioning that bar migration can be hindered by the presence of forcing effects such as instream obstacles, channel bends or uneven boundary conditions. These effects are expected to be particularly important when the channel is wide enough to exceed the so-called resonant conditions (Zolezzi & Seminara, 2001). In this case, any small but persistent asymmetry (e.g., in the upstream boundary condition) is expected to produce a spatially-growing disturbance that may disrupt bar migration. For example, Lanzoni (2000) suggested that steady bars can be triggered by the asymmetrical feeding of the recirculated sediment, while in the field-scale experiment by Venditti et al. (2012) bars were forced by an upstream flow constriction. Our results confirm this behavior when compared to the experiments of Redolfi et al. (2020), who used uniform sediment under similar flume conditions. In their case, bar migration occurred in all runs except when discharge was considerably low and bar crests partially emerged. In contrast, our experiments with sediment mixtures showed no migration, even when bars remained fully submerged (see all cases with $W_w/W = 1$ in Table 1).

The bar height, when normalized by the average water depth, shows values comparable to those reported by Redolfi et al. (2020), ranging from two to four times the average depth, and increasing under lower discharge conditions, when the width-to-depth ratio is larger. In contrast, the bar wavelength exhibits an unexpected trend, increasing with discharge. This behavior differs from previous studies (e.g., Jaeggi, 1984; Kinoshita, 1961; Redolfi, 2021; Redolfi et al., 2020; Sukegawa, 1972), which typically reported a decrease in bar wavelength with increasing discharge. Furthermore, the observed bar wavelength, when normalized by channel width, is notably large, ranging from 9 to 17 times the channel width, compared with the more common range of 5–10 channel widths documented for free alternate bars (e.g., Fujita & Muramoto, 1985; Jaeggi, 1984; Sukegawa, 1972). The observed larger values of L/W may be attributed to the reduction in migration rate, as the measured wavelengths approach those of steady "forced bars", which are typically about twice as long as free bars (e.g., Siviglia et al., 2013; Tubino et al., 1999). From this perspective, the influence of grain sorting on bar wavelength appears twofold: (a) it is expected to decrease the initial wavelength of migrating bars; and (b) it can halt bar migration, leading to marked bar elongation.

Moreover, the trend of bar wavelength with the width-to-depth ratio can be further interpreted on the basis of Figure 14a, which shows that the scaling length $C_0^2 D_0$ yields nearly constant values of L^*. Consequently, as channel width increases relative to flow depth (i.e., increasing β), L/W is expected to decrease, consistent with the trend in Figure 14b. It should also be noted that while the scaling length $C_0^2 D_0$ naturally arises in analyses of steady bar formation that neglect free surface deformation (Camporeale et al., 2007; Struiksma et al., 1985), this approach is not suitable for studying the initial wavelength selection of migrating bars, where Froude-dependent free surface effects play a relevant role (Redolfi, 2021).

The relatively large values of L/W we observed appear in contrast with previous experiments, in which sediment heterogeneity produced no significant effect or even a decrease in wavelength (Lanzoni, 2000). This suggests that the lack of sediment transport over bar tops introduces an internal forcing mechanism, preventing migration and producing bar elongation. In this case, the forcing is internal, and caused by the bar growth, in contrast to typical external forcing effects such as channel curvature, channel widening, or instream obstacles. In this respect, Redolfi et al. (2020) reported a similarly long bar wavelength in the case of an emerged bar pattern, with a uniform sediment distribution. Further investigation is needed to distinguish the relative roles of sediment heterogeneity and bar emergence in driving these elongation effects.

4.4. Availability of Spatially Distributed Data for Modeling Purposes

Mathematical and numerical models have been extensively used to investigate river bar morphodynamics and sediment sorting patterns. However, their parametrization remains challenging, particularly when simulating sediment mixtures. Specifically, the resulting sorting patterns are found to depend considerably on whether the drag coefficient is assumed to be uniform or allowed to spatially vary with local bed roughness (Nelson et al., 2015b), as well as on the parametrization of the hiding effect on bedload transport over a sloping bed (Ragno et al., 2023). Moreover, the mathematical nature of sorting equations can lead to issues of well-posedness and numerical accuracy, potentially limiting their ability to fully reproduce sorting patterns (Chavarrías et al., 2018). Similarly, the stochastic nature of sediment transport can make local application of deterministic transport models problematic (Ancey, 2020; Kleinhans & van Rijn, 2002). The availability of spatially distributed data, such as that obtained in this study, provides an opportunity to refine and validate mathematical models. For example, the observed phase lag may be used to directly test the ability of models to reproduce sorting pattern, at least under controlled hydraulic conditions. Finally, the use of two-dimensional spatial correlations between bed topography and grain size maps proved to be a robust tool for estimating the wavelengths of complex bar units, offering insights that cannot be captured by pointwise correlations alone.

4.5. The Relevance of Bar Sorting Patterns

The observed variability in topography and surface texture significantly influences sediment transport and downstream fining processes (e.g., Toro-Escobar et al., 2000). As highlighted by Paola and Seal (1995), the variability in bed shear stress and grain size associated with alternating bars enhances overall sediment transport rates and mobility differences among sediment grain size classes. Specifically, spatial variations are found to enhance differences in mobility between fine and coarse particles. Although this effect may be mitigated in cases where a positive correlation exists between bed shear stress and grain size (Paola & Seal, 1995), our experiments do not exhibit such a correlation. As a result, the observed spatial variability is expected to play a significant role in driving downstream fining processes through selective transport.

This variability also has ecological implications. Sorting patterns play an important role in determining habitat suitability for aquatic organisms. Specifically, the wide distributions of bed shear stress and grain size, and the lack of a direct correlation between them, can generate a large variety of physical habitat conditions. Coarse substrates with low bed shear stress, for instance, may serve as critical spawning grounds for fish species or as refugia for benthic organisms during high-flow events (e.g., Diplas & Parker, 1985; Kondolf, 2000; Lisle & Hilton, 1999).

4.6. Limitations and Future Perspectives

This study focused on a limited grain size range, corresponding to relatively fine to coarse gravel in gravel-bed rivers. For example, considering our experiment as a 1:40 Froude-scaled model of an ideal prototype river, our 0.5–2 mm range corresponds to 20–80 mm, in a channel 16–24 m wide, subject to a formative discharge ranging from 17 to 49 m^3/s. Therefore, our experiments cannot capture the behavior of sand deposits often observed in natural settings (e.g., Lisle & Hilton, 1999; Wathen et al., 1995). Additionally, the sediment mixture was only moderately sorted, with a Folk and Ward (1957) sorting coefficient of approximately 0.8. Poorer sorting distributions could result in stronger sorting effects and more rapid bar emergence. It is also worth mentioning that, despite preserving Froude and Shields numbers, undistorted laboratory models of river morphodynamics also produce reduced Reynolds numbers relative to the ideal prototype, which can affect flow resistance and sediment transport processes when viscous effects near the bed become dominant (Young & Warburton, 1996). However, since in our experiments the dimensionless particle size remained greater than approximately 10, these scale effects are assumed to play a secondary role (e.g., Lanzoni, 2000).

To isolate sorting effects driven by internal mechanisms, we also intentionally considered steady discharge. Therefore, we could not reproduce the effects of flow unsteadiness (Laronne & Reid, 1993) and variations in sediment supply (e.g., Bankert & Nelson, 2018; Hassan et al., 2023; Miwa et al., 2007; Venditti et al., 2012). Moreover, the interpretation of our experiments does not account for factors present in natural rivers, such as vegetation growth, exposure of bedrock, channel curvature, and geometric discontinuities that are likely to influence bed topography and sorting patterns. Future work should explore these effects to develop a more comprehensive understanding of sediment sorting under natural conditions.

Finally, the present analysis is based on the equilibrium state of bed and grain size arrangement and considers only bar-scale averaged parameters. Therefore, it does not allow reconstruction of time-dependent processes, such as the transient phase of bar development from the initially-flat bed. Further analysis based on recent experimental techniques (e.g., Moteki et al., 2022) could provide a more detailed description of the topography and grain sorting patterns, and may also help explain the differences among individual bars observed even in a regular flume.

5. Conclusion

This study provides a detailed analysis of surface grain size patterns on alternate bars at equilibrium in a straight channel with fixed banks and constant water and sediment supply. Using image analysis techniques we obtained high-resolution maps of the median grain size of the bed surface. In addition, simulations with a 2-D fixed-bed numerical model complemented the data set by providing flow field and bed shear stress information. The data were processed to reconstruct an average bar configuration and to explore spatial correlations through a 2-D analysis. The median grain size displays regular spatial patterns resembling those of the alternate bars. However, point-by-point correlations with bed elevation and shear stress are negligible.

The main novelty of our study lies in the identification of a systematic sorting pattern along alternate bars across multiple laboratory experiments, characterized by an upstream shift of about one quarter of the bar wavelength with respect to the bar topography. Coarser patches are consistently located just upstream of the crest, whereas fine patches are found on the lee side, upstream of the bar pool. This sorting pattern is largely independent of formative discharge and channel width, at least within the range of conditions tested in this study. The occurrence of these patterns can be interpreted considering that:

- Bed shear stress is shifted further upstream relative to the bed topography, with a phase lag of approximately $-3/4\pi$, thus showing also a spatial lag relative to the median grain size.
- The observed sediment sorting significantly affects bar dynamics, by suppressing sediment transport over the bar crest, effectively halting bar migration and transforming the bar into a fixed bedform. This process also results in a noticeable increase in bar wavelength compared to bars formed under similar conditions but with uniform sediments.
- Alternate bars can thus be regarded as *sorting-influenced* bedforms, in which the development of grain size patterns is not essential for their formation but can significantly affect their average properties, such as height, wavelength, and migration speed.
- Although these bars form freely from the inherent instability of the flow-sediment interaction, they eventually exhibit characteristics of forced (hybrid) bars, in terms of wavelength and (lack of) migration. This behavior is likely driven by the lack of sediment transport over the top portion of the bar, which creates a form of internal forcing.

The lack of systematic, high-resolution data in controlled environments has often limited a thorough validation of mathematical and numerical models and the empirical formulations used to describe the transport of different grain size fractions under the influence of flow and gravitational forces. The results presented here will be used in the companion paper (Ragno & Redolfi, 2026) to validate a 2-D mathematical model reproducing sorting patterns on steady alternate bars, highlighting the importance of accurately representing the effects of lateral slope. Similarly, these experimental findings, along with the associated data sets, provide a valuable foundation for investigating other key relevant factors, such as flow variability and changes in sediment supply.

Conflict of Interest

The authors declare no conflicts of interest relevant to this study.

Availability Statement

All maps of bed elevation, grain size, orthophotos as well as shear stress and flow velocity (Redolfi et al., 2025) are publicly available at https://doi.org/10.5281/zenodo.17306079.

Acknowledgments
This work has been partially carried out within the projects "SEDMORNET" funded by the European Union Next-GenerationEU (Piano Nazionale di Ripresa e Resilienza PNRR) - Mission 4 - Component C2 - Investment Fund 1.1 "Fondo per il Programma Nazionale di Ricerca e Progetti di Rilevante Interesse Nazionale (PRIN)", the project DICAM-EXC (Departments of Excellence 2023–2027, Grant L232/2016), and the Grant FAR-DIP-2024-REDOLFI funded by the University of Modena and Reggio Emilia. The laboratory experiments were supported by the project GLORI, funded by the Autonomous Province of Bolzano-Bozen. We thank Francesco Boari, Michele Portogallo, and the staff of the Hydraulic Laboratory for their help in the execution of the experiments. This paper has benefited from the comments of the Associate Editor, as well as those of Peter Nelson and two anonymous reviewers. Open access publishing facilitated by Universita degli Studi di Modena e Reggio Emilia, as part of the Wiley - CRUI-CARE agreement.

References

Alexander, J., & Fielding, C. (1997). Gravel antidunes in the tropical Burdekin River, Queensland, Australia. *Sedimentology*, *44*(2), 327–337. https://doi.org/10.1111/j.1365-3091.1997.tb01527.x

Ancey, C. (2020). Bedload transport: A walk between randomness and determinism. Part 1. The state of the art. *Journal of Hydraulic Research*, *58*(1), 1–17. https://doi.org/10.1080/00221686.2019.1702594

Ashmore, P., & Gardner, J. T. (2008). Unconfined confluences in braided rivers. In *River confluences, tributaries and the fluvial network* (pp. 119–147). John Wiley and Sons, Ltd. https://doi.org/10.1002/9780470760383.ch7

Ashworth, P., & Ferguson, R. (1986). Interrelationships of channel processes, changes and sediments in a proglacial braided river. *Geografiska Annaler - Series A: Physical Geography*, *68*(4), 361–371. https://doi.org/10.1080/04353676.1986.11880186

Ashworth, P., Ferguson, R. I., Ashmore, P. E., Paola, C., Powell, D. M., & Prestegaard, K. L. (1992). Measurements in a braided river chute and lobe 2. Sorting of bed load during entrainment, transport, and deposition. *Water Resources Research*, *28*(7), 1887–1896. https://doi.org/10.1029/92WR00702

Bankert, A. R., & Nelson, P. A. (2018). Alternate bar dynamics in response to increases and decreases of sediment supply. *Sedimentology*, *65*(3), 702–720. https://doi.org/10.1111/sed.12399

Bluck, B. (1971). Sedimentation in the meandering river endrick. *Scottish Journal of Geology*, *7*(2), 93–138. https://doi.org/10.1144/sjg07020093

Buffington, J. M., & Montgomery, D. R. (1999). A procedure for classifying textural facies in gravel-bed rivers. *Water Resources Research*, *35*(6), 1903–1914. https://doi.org/10.1029/1999WR900041

Callander, R. A. (1969). Instability and river channels. *Journal of Fluid Mechanics*, *36*(3), 465–480. https://doi.org/10.1017/S0022112069001765

Camporeale, C., Perona, P., Porporato, A., & Ridolfi, L. (2007). Hierarchy of models for meandering rivers and related morphodynamic processes. *Reviews of Geophysics*, *45*(1), 1–28. https://doi.org/10.1029/2005RG000185

Chavarrías, V., Stecca, G., & Blom, A. (2018). Ill-posedness in modeling mixed sediment river morphodynamics. *Advances in Water Resources*, *114*, 219–235. https://doi.org/10.1016/j.advwatres.2018.02.011

Claude, N., Rodrigues, S., Bustillo, V., Bréhéret, J.-G., Tassi, P., & Jugé, P. (2014). Interactions between flow structure and morphodynamic of bars in a channel expansion/contraction, Loire River, France. *Water Resources Research*, *50*(4), 2850–2873. https://doi.org/10.1002/2013WR015182

Colombini, M., & Parker, G. (1995). Longitudinal streaks. *Journal of Fluid Mechanics*, *304*, 161–183. https://doi.org/10.1017/S0022112095004381

Colombini, M., Seminara, G., & Tubino, M. (1987). Finite-amplitude alternate bars. *Journal of Fluid Mechanics*, *181*(HY9), 213–232. https://doi.org/10.1017/S0022112087002064

Cordier, F., Tassi, P., Claude, N., Crosato, A., Rodrigues, S., & Pham Van Bang, D. (2019). Numerical study of alternate bars in alluvial channels with nonuniform sediment. *Water Resources Research*, *55*(4), 2976–3003. https://doi.org/10.1029/2017WR022420

Diplas, P., & Parker, G. (1985). Pollution of gravel spawning grounds due to fine sediment. In *Project Report-University of Minnesota*. St. Anthony Falls Hydraulic Laboratory.

Folk, R. L., & Ward, W. C. (1957). Brazos river bar: A study in the significance of grain size parameters. *Journal of Sedimentary Research*, *27*(1), 3–26. https://doi.org/10.1306/74D70646-2B21-11D7-8648000102C1865D

Fredsoe, J. (1978). Meandering and braiding of rivers. *Journal of Fluid Mechanics*, *84*(November), 609–624. https://doi.org/10.1017/S0022112078000373

Fujita, Y., & Muramoto, Y. (1985). Studies on the process of development of alternate bars. *Bulletin of the Disaster Prevention Research Institute*, *35*(3), 55–86.

García, M. H. (2008). Sediment transport and morphodynamics. In *Sedimentation engineering* (pp. 21–163). ASCE. https://doi.org/10.1061/9780784408148.ch02

Garcia, X.-F., Schnauder, I., & Pusch, M. T. (2012). Complex hydromorphology of meanders can support benthic invertebrate diversity in rivers. *Hydrobiologia*, *685*(1), 49–68. https://doi.org/10.1007/s10750-011-0905-z

Gardner, J. T., & Ashmore, P. E. (2011). Geometry and grain-size characteristics of the basal surface of a braided river deposit. *Geology*, *39*(3), 247–250. https://doi.org/10.1130/G31639.1

Guerit, L., Barrier, L., Narteau, C., Métivier, F., Liu, Y., Lajeunesse, E., et al. (2014). The grain-size patchiness of braided gravel-bed streams—Example of the Urumqi River (northeast Tian Shan, China). *Advances in Geosciences*, *37*, 27–39. https://doi.org/10.5194/adgeo-37-27-2014

Gurnell, A. M., Petts, G. E., Hannah, D. M., Smith, B. P. G., Edwards, P. J., Kollmann, J., et al. (2001). Riparian vegetation and island formation along the gravel-bed Fiume Tagliamento, Italy. *Earth Surface Processes and Landforms*, *26*(1), 31–62. https://doi.org/10.1002/1096-9837(200101)26:1⟨31::AID-ESP155⟩3.0.CO;2-Y

Hassan, M. A., Chartrand, S. M., Radić, V., Ferrer-Boix, C., Buckrell, E., & McDowell, C. (2022). Experiments on the sediment transport along pool-riffle unit. *Water Resources Research*, *58*(9), 1–23. https://doi.org/10.1029/2022wr032796

Hassan, M. A., Li, W., Viparelli, E., An, C., & Mitchell, A. J. (2023). Influence of sediment supply timing on bedload transport and bed surface texture during a single experimental hydrograph in gravel bed rivers. *Water Resources Research*, *59*(12), e2023WR035406. https://doi.org/10.1029/2023WR035406

Hodge, R. A., Sear, D. A., & Leyland, J. (2013). Spatial variations in surface sediment structure in riffle–pool sequences: A preliminary test of the Differential Sediment Entrainment Hypothesis (DSEH). *Earth Surface Processes and Landforms*, *38*(5), 449–465. https://doi.org/10.1002/esp.3290

Ikeda, S., Yamasaka, M., & Chiyoda, M. (1987). Bed topography and sorting in bends. *Journal of Hydraulic Engineering*, *113*(2), 190–204. https://doi.org/10.1061/(asce)0733-9429(1987)113:2(190)

Jaeggi, M. N. R. (1984). Formation and effects of alternate bars. *Journal of Hydraulic Engineering*, *110*(2), 142–156. https://doi.org/10.1061/(asce)0733-9429(1984)110:2(142)

Javernick, L., Redolfi, M., & Bertoldi, W. (2018). Evaluation of a numerical model's ability to predict bed load transport observed in braided river experiments. *Advances in Water Resources*, *115*, 207–218. https://doi.org/10.1016/j.advwatres.2018.03.012

Julien, P. Y., & Anthony, D. J. (2002). Bed load motion and grain sorting in a meandering stream. *Journal of Hydraulic Research*, *40*(2), 125–133. https://doi.org/10.1080/00221680209499855

Keulegan, G. H. (1938). Laws of turbulent flow in open channels. *Journal of Research of the National Bureau of Standards*, *21*(6), 707–741. https://doi.org/10.6028/jres.021.039

Kinoshita, R. (1961). Investigation of channel deformation in Ishikari River. *Report of Bureau of Resources, Dept. Science and Technology, Japan, 174*. Publisher: Department of Science and Technology.

Kleinhans, M. G., & van Rijn, L. C. (2002). Stochastic prediction of sediment transport in sand-gravel bed rivers. *Journal of Hydraulic Engineering*, *128*(4), 412–425. https://doi.org/10.1061/(ASCE)0733-9429(2002)128:4(412)

Kondolf, G. M. (2000). Assessing salmonid spawning gravel quality. *Transactions of the American Fisheries Society*, *129*(1), 262–281. https://doi.org/10.1577/1548-8659(2000)129⟨0262:ASSGQ⟩2.0.CO;2

Lanzoni, S. (2000). Experiments on bar formation in a straight flume 2. Graded sediment. *Water Resources Research*, *36*(11), 3351–3363. https://doi.org/10.1029/2000WR900160

Lanzoni, S., & Tubino, M. (1999). Grain sorting and bar instability. *Journal of Fluid Mechanics*, *393*, 149–174. https://doi.org/10.1017/S0022112099005583

Laronne, J. B., & Reid, I. (1993). Very high rates of bedload sediment transport by ephemeral desert rivers. *Nature*, *366*(6451), 148–150. https://doi.org/10.1038/366148a0

Leduc, P., Ashmore, P., & Gardner, J. T. (2015). Grain sorting in the morphological active layer of a braided river physical model. *Earth Surface Dynamics*, *3*(4), 577–585. https://doi.org/10.5194/esurf-3-577-2015

Lewin, J. (1976). Initiation of bed forms and meanders in coarse-grained sediment. *Geological Society of America Bulletin*, *87*(2), 281. https://doi.org/10.1130/0016-7606(1976)87⟨281:IOBFAM⟩2.0.CO;2

Lisle, T. E., & Hilton, S. (1999). Fine bed material in pools of natural gravel bed channels. *Water Resources Research*, *35*(4), 1291–1304. https://doi.org/10.1029/1998WR900088

Lisle, T. E., Ikeda, H., & Iseya, F. (1991). Formation of stationary alternate bars in a steep channel with mixed-size sediment: A flume experiment. *Earth Surface Processes and Landforms*, *16*(5), 463–469. https://doi.org/10.1002/esp.3290160507

Lisle, T. E., & Madej, M. A. (1992). Spatial variation in armouring in a channel with high sediment supply. In P. Billi, R. D. Hey, C. R. Thorne, & P. Tacconi (Eds.), *Dynamics of gravel-bed Rivers* (pp. 277–293). John Wiley and Sons Ltd.

Lisle, T. E., Nelson, J. M., Pitlick, J., Madej, M. A., & Barkett, B. L. (2000). Variability of bed mobility in natural, gravel-bed channels and adjustments to sediment load at local and reach scales. *Water Resources Research*, *36*(12), 3743–3755. https://doi.org/10.1029/2000WR900238

Lunt, I. A., & Bridge, J. S. (2004). Evolution and deposits of a gravelly braid bar, Sagavanirktok River, Alaska. *Sedimentology*, *51*(3), 415–432. https://doi.org/10.1111/j.1365-3091.2004.00628.x

MacKenzie, L. G., Eaton, B. C., & Church, M. (2018). Breaking from the average: Why large grains matter in gravel-bed streams. *Earth Surface Processes and Landforms*, *43*(15), 3190–3196. https://doi.org/10.1002/esp.4465

Milne, J. A. (1982). Bed-material size and the riffle-pool sequence. *Sedimentology*, *29*(2), 267–278. https://doi.org/10.1111/j.1365-3091.1982.tb01723.x

Miwa, H., Daido, A., & Katayama, T. (2007). Effects of water and sediment discharge conditions on variation in alternate bar morphology. *Proceedings of Hydraulic Engineering*, *51*, 1051–1056. https://doi.org/10.2208/prohe.51.1051

Mosley, M. P., & Tindale, D. S. (1985). Sediment variability and bed material sampling in gravel-bed rivers. *Earth Surface Processes and Landforms*, *10*(5), 465–482. https://doi.org/10.1002/esp.3290100506

Moteki, D., Murai, T., Hoshino, T., Yasuda, H., Muramatsu, S., & Hayasaka, K. (2022). Capture method for digital twin of formation processes of sand bars. *Physics of Fluids*, *34*(3), 034117. https://doi.org/10.1063/5.0085574

Nelson, P. A., Dietrich, W. E., & Venditti, J. G. (2010). Bed topography and the development of forced bed surface patches. *Journal of Geophysical Research*, *115*(4), 1–19. https://doi.org/10.1029/2010JF001747

Nelson, P. A., McDonald, R. R., Nelson, J. M., & Dietrich, W. E. (2015a). Coevolution of bed surface patchiness and channel morphology: 1. Mechanisms of forced patch formation. *Journal of Geophysical Research: Earth Surface*, *120*(9), 1687–1707. https://doi.org/10.1002/2014JF003428

Nelson, P. A., McDonald, R. R., Nelson, J. M., & Dietrich, W. E. (2015b). Coevolution of bed surface patchiness and channel morphology: 2. Numerical experiments. *Journal of Geophysical Research F: Earth Surface*, *120*(9), 1708–1723. https://doi.org/10.1002/2014JF003429

Nelson, P. A., & Morgan, J. A. (2018). Flume experiments on flow and sediment supply controls on gravel bedform dynamics. *Geomorphology*, *323*, 98–105. https://doi.org/10.1016/j.geomorph.2018.09.011

Nelson, P. A., Venditti, J. G., Dietrich, W. E., Kirchner, J. W., Ikeda, H., Iseya, F., & Sklar, L. S. (2009). Response of bed surface patchiness to reductions in sediment supply. *Journal of Geophysical Research*, *114*(F2), 2008JF001144. https://doi.org/10.1029/2008JF001144

Paola, C., & Seal, R. (1995). Grain size patchiness as a cause of selective deposition and downstream fining. *Water Resources Research*, *31*(5), 1395–1407. https://doi.org/10.1029/94wr02975

Parker, G. (1976). On the cause and characteristic scales of meandering and braiding in rivers. *Journal of Fluid Mechanics*, *76*(3), 457–480. https://doi.org/10.1017/s0022112076000748

Parker, G. (2008). Transport of gravel and sediment mixtures. In M. H. García (Ed.), *Sedimentation engineering* (pp. 165–251). ASCE. https://doi.org/10.1061/9780784408148.ch03

Parker, G., & Andrews, E. D. (1985). Sorting of bed load sediment by flow in meander bends. *Water Resources Research*, *21*(9), 1361–1373. https://doi.org/10.1029/WR021i009p01361

Powell, D. M. (1998). Patterns and processes of sediment sorting in gravel-bed rivers. *Progress in Physical Geography*, *22*(1), 1–32. https://doi.org/10.1177/030913339802200101

Qian, H., Cao, Z., Liu, H., & Pender, G. (2017). Numerical modelling of alternate bar formation, development and sediment sorting in straight channels. *Earth Surface Processes and Landforms*, *42*(4), 555–574. https://doi.org/10.1002/esp.3988

Ragno, N., & Redolfi, M. (2026). Grain size sorting and steady bars formation in straight channels—Part 2: Linear theory. *Journal of Geophysical Research: Earth Surface*. https://doi.org/10.1029/2025JF008576

Ragno, N., Redolfi, M., Tambroni, N., & Tubino, M. (2023). Modeling steady grain sorting in river bifurcations. *Journal of Geophysical Research: Earth Surface*, *128*(9), e2023JF007230. https://doi.org/10.1029/2023JF007230

Ragno, N., Redolfi, M., & Tubino, M. (2022). Quasi-universal length scale of river anabranches. *Geophysical Research Letters*, *49*(16), 1–9. https://doi.org/10.1029/2022GL099928

Ragno, N., Tambroni, N., & Bolla Pittaluga, M. (2021). When and where do free bars in estuaries and tidal channels form? *Journal of Geophysical Research: Earth Surface*, *126*(10), e2021JF006196. https://doi.org/10.1029/2021JF006196

Redolfi, M. (2021). Free alternate bars in rivers: Key physical mechanisms and simple formation criterion. *Water Resources Research*, *57*(12), e2021WR030617. https://doi.org/10.1029/2021wr030617

Redolfi, M., Ragno, N., Matilde, W., & Bertoldi, W. (2025). Laboratory data of bed topography, grain size, water depth and flow velocity along alternate bars [Dataset]. *Zenodo*. https://doi.org/10.5281/zenodo.17306079

Redolfi, M., Welber, M., Carlin, M., Tubino, M., & Bertoldi, W. (2020). Morphometric properties of alternate bars and water discharge: A laboratory investigation. *Earth Surface Dynamics*, *8*(3), 1–31. https://doi.org/10.5194/esurf-2020-27

Rice, S. P., & Church, M. (2010). Grain-size sorting within river bars in relation to downstream fining along a wandering channel. *Sedimentology*, *57*(1), 232–251. https://doi.org/10.1111/j.1365-3091.2009.01108.x

Rubin, D. M. (2004). A simple autocorrelation algorithm for determining grain size from digital images of sediment. *Journal of Sedimentary Research*, *74*(1), 160–165. https://doi.org/10.1306/052203740160

Seminara, G. (1995). Effect of grain sorting on the formation of bedforms. *Applied Mechanics Reviews*, *48*(9), 549–563. https://doi.org/10.1115/1.3023144

Seminara, G. (2010). Fluvial sedimentary patterns. *Annual Review of Fluid Mechanics*, *42*(1), 43–66. https://doi.org/10.1146/annurev-fluid-121108-145612

Seminara, G., Colombini, M., & Parker, G. (1996). Nearly pure sorting waves and formation of bedload sheets. *Journal of Fluid Mechanics*, *312*(April), 253–278. https://doi.org/10.1017/S0022112096001991

Seminara, G., & Tubino, M. (2001). Sand bars in tidal channels. Part 1. Free bars. *Journal of Fluid Mechanics*, *440*, 49–74. https://doi.org/10.1017/S0022112001004748

Siviglia, A., Stecca, G., Vanzo, D., Zolezzi, G., Toro, E. F., & Tubino, M. (2013). Numerical modelling of two-dimensional morphodynamics with applications to river bars and bifurcations. *Advances in Water Resources*, *52*, 243–260. https://doi.org/10.1016/j.advwatres.2012.11.010

Storz-Peretz, Y., & Laronne, J. B. (2013). Morphotextural characterization of dryland braided channels. *Geological Society of America Bulletin*, *125*(9–10), 1599–1617. https://doi.org/10.1130/B30773.1

Struiksma, N., & Crosato, A. (1989). Analysis of a 2-D bed topography model for rivers. In S. Ikeda & G. Parker (Eds.), *River meandering* (pp. 153–180). https://doi.org/10.1029/wm012p0153

Struiksma, N., Olesen, K. W., Flokstra, C., & De Vriend, H. J. (1985). Bed deformation in curved alluvial channels. *Journal of Hydraulic Research*, *23*(1), 57–79. https://doi.org/10.1080/00221688509499377

Sukegawa, N. (1972). Criterion for alternate bar formation in experimental flumes. *Proc Jap Soc Civ Eng*, *207*, 47–50. https://doi.org/10.2208/jscej1969.1972.207_47

Takebayashi, H., & Egashira, S. (2001). Dynamic state of sand bar formed on non-uniform sediment bed. *Proceedings of JSCE*, *45*, 727–732. https://doi.org/10.2208/prohe.45.727

Tockner, K., Paetzold, A., Karaus, U., Claret, C., & Zettel, J. (2006). *Ecology of braided rivers* (Vol. 36). Special Publication-International Association of Sedimentologists.339.

Toro-Escobar, C. M., Paola, C., Parker, G., Wilcock, P. R., & Southard, J. B. (2000). Experiments on downstream fining of gravel: II. Wide and sandy runs. *Journal of Hydraulic Engineering*, *126*(3), 198–208. https://doi.org/10.1061/(asce)0733-9429(2000)126:3(198)

Tubino, M., Repetto, R., & Zolezzi, G. (1999). Free bars in rivers. *Journal of Hydraulic Research*, *37*(6), 759–775. https://doi.org/10.1080/00221689909498510

Vanzo, D., Peter, S., Vonwiller, L., Bürgler, M., Weberndorfer, M., Siviglia, A., et al. (2021). Basement v3: A modular freeware for river process modelling over multiple computational backends. *Environmental Modelling and Software*, *143*, 105102. https://doi.org/10.1016/j.envsoft.2021.105102

Venditti, J. G., Nelson, P. A., Minear, J. T., Wooster, J., & Dietrich, W. E. (2012). Alternate bar response to sediment supply termination. *Journal of Geophysical Research*, *117*(F2), 2011JF002254. https://doi.org/10.1029/2011JF002254

Ward, J. V., Tockner, K., Arscott, D. B., & Claret, C. (2002). Riverine landscape diversity. *Freshwater Biology*, *47*(4), 517–539. https://doi.org/10.1046/j.1365-2427.2002.00893.x

Wathen, S. J., Ferguson, R. I., Hoey, T. B., & Werritty, A. (1995). Unequal mobility of gravel and sand in weakly bimodal river sediments. *Water Resources Research*, *31*(8), 2087–2096. https://doi.org/10.1029/95WR01229

White, D. C., & Nelson, P. A. (2023). Flume investigation into mechanisms responsible for particle sorting in gravel-bed meandering channels. *Journal of Geophysical Research: Earth Surface*, *128*, 1–17. https://doi.org/10.1029/2022JF006821

Whiting, P. J., Dietrich, W. E., Leopold, L. B., Drake, T. G., & Shreve, R. L. (1988). Bedload sheets in heterogeneous sediment. *Geology*, *16*(2), 105–108. https://doi.org/10.1130/0091-7613(1988)016⟨0105:BSIHS⟩2.3.CO;2

Wilcock, P. R., & Crowe, J. C. (2003). Surface-based transport model for mixed-size sediment. *Journal of Hydraulic Engineering*, *129*(February), 120–128. https://doi.org/10.1061/(ASCE)0733-9429(2003)129:2(120)

Young, W. J., & Warburton, J. (1996). Principles and practice of hydraulic modelling of braided gravel-bed rivers. *Journal of Hydrology New Zealand*, *35*(2), 175–198. https://doi.org/10.1016/S0301-9322(97)80098-5

Zolezzi, G., & Seminara, G. (2001). Downstream and upstream influence in river meandering. Part 1. General theory and application to overdeepening. *Journal of Fluid Mechanics*, *438*(July), 183–211. https://doi.org/10.1017/S0022112001004281